Ref. Ares(2026)7831399 - 12/08/2026

EU MISSIONS
RESTORE OUR OCEAN AND WATERS

Scalable full-cycle marine litter remediation in the Mediterranean: Robotic and participatory solutions

SeaClear 2.0

https://www.seaclear2.eu

D5.1
Report on UAV, USV and ROV control upgrade
WP5 — Control Overhaul

Grant Agreement no. 101093822

Lead beneficiary: UNIDU

Date: 30/06/2025
Type: R
Dissemination level: PU

Document information

Grant agreement no.	101093822
Acronym:	SeaClear2.0
Full title:	Scalable full-cycle marine litter remediation in the Mediterranean: Robotic and participatory solutions
Start date of the project	01/01/2023
Duration of the project	48 months
Deliverable	D5.1: Report on UAV, USV and ROV control upgrade
Work package	WP5: Control Overhaul
Deliverable leader	UNIDU
Delivery date	Contractual: 30/04/2025 Actual: 30/06/2025
Status	Draft ☐ Final ✓
Type[1]	R ✓ DEM ☐ OTHER ☐ DMP ☐
Dissemination level[2]	PU ✓ C-UE/EU-C ☐ SEN ☐
Author(s)	Ivana Palunko (University of Dubrovnik) Stefan Sosnowski (Technical University Munich) Gianpietro Battocletti (Technical University Delft) Lucian Busoniu (Universitatea Tehnica Cluj-Napoca)
Ivana Palunko, email: ivana.palunko@unidu.hr	Cosmin Delea (Fraunhofer) **Responsible author** University of Dubrovnik
Deliverable description	Report on UAV, USV and ROV control upgrade (<=T5.1)

[1]R = Document, report, DEM = demonstrator, OTHER: Software, technical diagram, etc. DMP = Data Management Plan
[2]PU = Public, C-UE/EU-C = EU Confidential under Decision 2015/444, SEN = Sensitive

Co-funded by the European Union

SeaClear2.0 is co-funded by the European Union under the Horizon Europe Programme (Grant Agreement 101093822). Views and opinions expressed herein are those of the author(s) and do not necessarily reflect those of the European Union or European Climate, Infrastructure and Environment Executive Agency (CINEA). Neither the European Union nor the granting authority can be held responsible for them

Co-funded by the European Union

SeaClear2.0 is co-funded by the European Union under the Horizon Europe Programme (Grant Agreement 101093822). Views and opinions expressed herein are those of the author(s) and do not necessarily reflect those of the European Union or European Climate, Infrastructure and Environment Executive Agency (CINEA). Neither the European Union nor the granting authority can be held responsible for them

Document history

Name	Date	Version	Description
Ivana Palunko	01/04/2025	V0.1	initial draft setup
Ivana Palunko	16/04/2025	V0.2	adds UAV and SeaBees control
Gianpietro Battocletti	18/04/2025	V0.3	adds SeaCat control
Stefan Sosnowski	16/06/2025	V0.4	adds grapple control
Lucian Busoniu	18/06/2025	V0.5	adds observation ROV control
Ivana Palunko	25/06/2025	V0.6	version for internal review
Ivana Palunko	27/06/2025	V1.0	final version
Cosmin Delea	03/07/2026	V1.1	adds SeaDragon control section

Co-funded by the European Union

SeaClear2.0 is co-funded by the European Union under the Horizon Europe Programme (Grant Agreement 101093822). Views and opinions expressed herein are those of the author(s) and do not necessarily reflect those of the European Union or European Climate, Infrastructure and Environment Executive Agency (CINEA). Neither the European Union nor the granting authority can be held responsible for them

Disclaimer of warranties

This document has been prepared by SeaClear2.0 project partners as an account of work carried out within the framework of Grant Agreement no. 101093822. Neither the Project Coordinator, nor any signatory party of the SeaClear2.0 Project Consortium Agreement, nor any person acting on behalf of any of them:

- makes any warranty or representation whatsoever, express or implied, with respect to the use of any information, apparatus, method, process, or similar item disclosed in this document, including merchantability and fitness for a particular purpose, that such use does not infringe on or interfere with privately owned rights, including any party's intellectual property; or
- makes any warranty or representation whatsoever, express or implied, that this document is suitable to any particular user's circumstance; or
- assumes responsibility for any damages or other liability whatsoever (including any consequential damages, even if the Project Coordinator or any representative of a signatory party of the Project Consortium Agreement, has been advised of the possibility of such damages) resulting from your selection or use of this document or any information, apparatus, method, process, or similar item disclosed in this document.

SeaClear2.0 is co-funded by the European Union under the Horizon Europe Programme (Grant Agreement 101093822). Views and opinions expressed are those of the author(s) and do not necessarily reflect those of the European Union or European Climate, Infrastructure and Environment Executive Agency (CINEA). Neither the European Union nor the granting authority can be held responsible for them.

Table of Contents

Definitions . . . 8

Abbreviations . . . 8

Executive Summary . . . 10

1 Introduction - SeaClear 2.0 at a Glance . . . 11

2 UAV control upgrade . . . 12
- 2.1 Modelling of tethered UAV . . . 12
  - 2.1.1 Newton-Euler equations . . . 16
- 2.2 Nonlinear Model Predictive Controller . . . 17
  - 2.2.1 Plant model . . . 17
  - 2.2.2 Controller formulation . . . 18
  - 2.2.3 Controller implementation . . . 19
- 2.3 Simulations . . . 21
- 2.4 Experimental Setup and Implementation Details . . . 21
  - 2.4.1 Experimental validation . . . 23
- 2.5 Conclusion . . . 24

3 USV control upgrade . . . 25
- 3.1 SeaCat control . . . 25
  - 3.1.1 Modelling of the SeaCat2.0 . . . 25
  - 3.1.2 Dynamic positioning controllers . . . 30
  - 3.1.3 Simulations . . . 31
  - 3.1.4 Conclusion . . . 31
- 3.2 SeaBees control . . . 34
  - 3.2.1 Modeling of Individual SeaBees . . . 34
  - 3.2.2 Model Predictive Control . . . 36
  - 3.2.3 Simulation Results . . . 37
  - 3.2.4 Conclusion . . . 38
- 3.3 SeaDragon control . . . 39
  - 3.3.1 USV hydrodynamic model . . . 39
  - 3.3.2 Autonomous docking procedure . . . 42
  - 3.3.3 Simulation results . . . 43
  - 3.3.4 Experimental results . . . 45
  - 3.3.5 Conclusions . . . 47

4 ROV control upgrade . . . 49
- 4.1 Observation ROV . . . 49
  - 4.1.1 Modelling of the observation ROV . . . 49
  - 4.1.2 LQT control for the observation ROV . . . 51
  - 4.1.3 Simulations using the LQT control strategy . . . 53
  - 4.1.4 Upgraded PID control . . . 53
  - 4.1.5 Novel experimental results . . . 55

4.2 Underwater Smart Grapple 55
4.2.1 Cascaded PID Control Formulation 56
4.2.2 Simulations 58
4.2.3 Experimental results 59

5 Conclusion 62

References 64

Co-funded by the European Union

SeaClear2.0 is co-funded by the European Union under the Horizon Europe Programme (Grant Agreement 101093822). Views and opinions expressed herein are those of the author(s) and do not necessarily reflect those of the European Union or European Climate, Infrastructure and Environment Executive Agency (CINEA). Neither the European Union nor the granting authority can be held responsible for them

Definitions

- **Beneficiary:** A legal entity that is signatory of the EC Grant Agreement no. 101093822.
- **Consortium:** The SeaClear2.0 Consortium, comprising the below-mentioned list of beneficiaries.
- **Consortium Agreement:** Agreement concluded amongst SeaClear2.0 Beneficiaries for the implementation of the Grant Agreement.
- **Grant Agreement:** The agreement signed between the beneficiaries and the EC for the undertaking of the SeaClear 2.0 project (Grant Agreement no. 101093822).

Beneficiaries of the SeaClear2.0 Consortium are referred to herein according to the following abbreviations:

- **TU Delft:** TECHNISCHE UNIVERSITEIT DELFT
- **DUNEA:** REGIONALNA AGENCIJA DUNEA
- **Fraunhofer:** FRAUNHOFER GESELLSCHAFT ZUR FORDERUNG DER ANGEWANDTEN FORSCHUNG EV
- **HPA:** HAMBURG PORT AUTHORITY
- **ISOTECH**: ISOTECH LTD
- **MDanchor**: M. DANCHOR LTD
- **Subsea Tech:** SUBSEA TECH SAS
- **TECNOSUB**: TÉCNICAS Y OBRAS SUBACUÁTICAS, SLU
- **TUM**: TECHNISCHE UNIVERSITAET MUENCHEN
- **UNIDU:** SVEUCILISTE U DUBROVNIKU
- **UTC**: UNIVERSITATEA TEHNICA CLUJ-NAPOCA
- **VEO**: VEOLIA PROPRETE
- **VLPF**: VENICE LAGOON PLASTIC FREE

Co-funded by the European Union

SeaClear2.0 is co-funded by the European Union under the Horizon Europe Programme (Grant Agreement 101093822). Views and opinions expressed herein are those of the author(s) and do not necessarily reflect those of the European Union or European Climate, Infrastructure and Environment Executive Agency (CINEA). Neither the European Union nor the granting authority can be held responsible for them

Abbreviations

DOF Degrees of Freedom. 25, 30, 39, 40, 47, 50, 56, 57

DP Dynamic Positioning. 25, 62

DVL Doppler Velocity Logger. 59–61

EKF Extended Kalman Filter. 57

ENU East-North-Up. 21, 23

EOM Equations of Motion. 39

GCS Ground Control Station. 21, 22

GNSS Global Navigation Satellite System. 45

GPS Global Positioning System. 22, 23, 56

LARS Launch and Recovery System. 12–15, 17, 19–24

LQT Linear Quadratic Tracking. 51–53, 62

MARUS MArine Robotic Unity Simulator. 62

MPC Model Predictive Control. 30, 31, 34, 36–38, 62

NMPC Nonlinear Model Predictive Control. 12, 20–24, 30, 31

PID Proportional-Integral-Derivative. 25, 30, 34, 56, 62

RIB Rigid Inflatable Boat. 45

ROS Robot Operating System. 21, 56

ROV Remotely Operated Vehicle. 10, 11, 49–53, 55, 56, 62

RTK Real-Time Kinematics. 20–23

SBL Short Baseline. 56

SQP Sequential Quadratic Programming. 21

TMS Tether Management System. 12

UAV Unmanned Aerial Vehicle. 10, 12–14, 17, 20–24, 62

USG Underwater Smart Grapple System. 10, 55, 56, 61, 62

USV Unmanned Surface Vehicle. 10–13, 15, 21, 24–31, 34–37, 39–43, 45, 47, 48, 55, 62

#MissionOcean #EUMissions #HorizonEU #OceanCharter

Co-funded by the European Union

SeaClear2.0 is co-funded by the European Union under the Horizon Europe Programme (Grant Agreement 101093822). Views and opinions expressed herein are those of the author(s) and do not necessarily reflect those of the European Union or European Climate, Infrastructure and Environment Executive Agency (CINEA). Neither the European Union nor the granting authority can be held responsible for them

Executive Summary

This document is part of the SeaClear 2.0 project, which aims to develop an autonomous robotic systems for marine litter collection. The report focuses on the advancements in control techniques for various robotic components used in the project, including Unmanned Aerial Vehicles (UAVs), Unmanned Surface Vehicles (USVs), Remotely Operated Vehicles (ROVs), and the Underwater Smart Grapple System (USG).

This document will detail the methodologies, system models, algorithm design, and experimental results related to control.

Key Points

1. **Theoretical Background** The document provides an overview of the theoretical principles for specific control structure of each individual SeaClear 2.0 subsystem.
2. **System Models** Detailed descriptions of the kinematic and dynamics models used for control design in surface vehicles (USVs), underwater vehicles (ROVs), and the aerial vehicles (UAVs), including hydrodynamic models
3. **Simulation/Experimental Results** The report presents the results of various simulation and experimental validation conducted to validate control algorithms. This includes:
   - Experimental validation of the SeaHawk, a tethered UAV cooperative control,
   - SeaCat2, USV reference tracking and DP control validated in simulation
   - SeaBees control validated in simulation, cooperative USV control
   - MiniTortuga ROV simulations to validate the optimal control strategy
   - A simulation-based evaluation of the cascaded control for the smart grapple system USG.
4. **Conclusion**

   The simulation and experimental results demonstrate the effectiveness of the proposed techniques and provide a foundation for further improvements and integration into the overall system.

Co-funded by the European Union

SeaClear2.0 is co-funded by the European Union under the Horizon Europe Programme (Grant Agreement 101093822). Views and opinions expressed herein are those of the author(s) and do not necessarily reflect those of the European Union or European Climate, Infrastructure and Environment Executive Agency (CINEA). Neither the European Union nor the granting authority can be held responsible for them

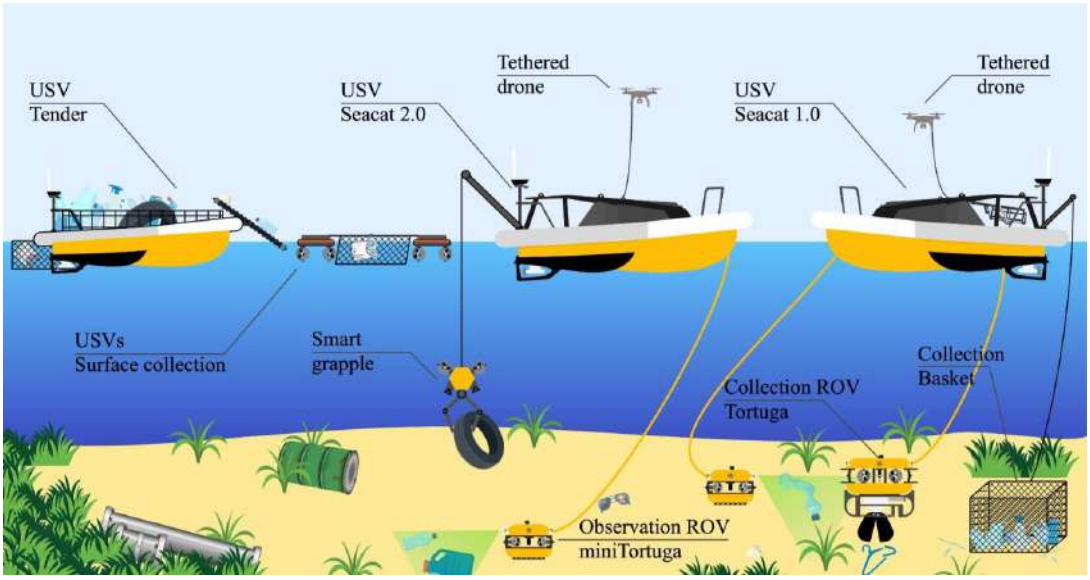


Figure 1: Concept of SeaClear 2.0 robotic system (left/middle) and SeaClear 1.0 (right)

1 Introduction - SeaClear 2.0 at a Glance

SeaClear 2.0 is the next step to the H2020-funded SeaClear (https://seaclear-project.eu), where several of the SeaClear2.0 partners have been developing the first autonomous robotic system for seafloor litter collection. An USV called SeaCAT acts as a hub for an unmanned aerial vehicle (UAV) that searches for litter from the air and contributes to situational awareness, an observation ROV called Mini-Tortuga that searches for litter underwater, and a collection ROV called Tortuga that collects the litter with a custom gripper plus-suction device and deposits it in a basket lowered from the USV. The very nature of SeaClear (labelled 1.0 in the document) as the first project to design such a solution means it must focus almost exclusively on technological developments in robotics hardware and algorithms, with a single system.

Moreover, the system is limited to only seafloor litter of up to tens of centimeters in size and at depths of up to tens of meters; it cannot collect surface litter or larger objects like fishing equipment, bikes, e-scooters, tires, shipping equipment, etc, which SeaClear 1.0 identified as a significant subset of the litter in industrial port or mariculture settings. The aim of SeaClear 2.0 is to upscale and upgrade the system initially made for SeaClear 1.0. This means collecting bigger and heavier litter with a modified SeaCAT2 and a smart grapple, storing and shipping it to shore with a dedicated USV Tender, as well as collecting surface litter with SeaBees a team of highly manoeuvrable surface robots. In the end, SeaClear 1.0 and SeaClear 2.0 will be working together, exploiting their shared and complementary litter detection and collection capabilities.

Co-funded by the European Union

SeaClear2.0 is co-funded by the European Union under the Horizon Europe Programme (Grant Agreement 101093822). Views and opinions expressed herein are those of the author(s) and do not necessarily reflect those of the European Union or European Climate, Infrastructure and Environment Executive Agency (CINEA). Neither the European Union nor the granting authority can be held responsible for them

2 UAV control upgrade

In this deliverable, we are reporting on coordinated control system for an autonomous tethered aerial vehicle system. This system is part of the SeaClear and SeaClear2.0 projects. An autonomous tethered aerial vehicle system includes two segments: an unmanned aerial vehicle UAV and its Launch and Recovery System Launch and Recovery System (LARS). The UAV-LARS is envisioned as a compact standalone unit that can be deployed from various platforms, such as ground vehicles, ships, or autonomous unmanned surface vehicles USVs like SeaCat, depicted in Fig. 2.

The UAV, a unidirectional-thrust multirotor platform, is tethered to the LARS, which provides power, communication, and a Tether Management System (TMS). In the proposed use case, the UAV is tasked with tracking the user-defined position reference relative to LARS mounted on a moving platform. At the same time, TMS regulates the tether interaction force to prevent excessive pull or, in contrast, excessive slack that can lead to entanglements. Consequently, the development of coordinated control is necessary to meet the end-user requirements and ensure operational safety.

To address the increased complexity arising from the coupled dynamics and strong nonlinearities of the tethered aerial system in the outlined use case, the control strategy based on the Nonlinear Model Predictive Control (NMPC) is proposed. Compared to classic methods, NMPC offers several key advantages, including the ability to impose constraints on system states and inputs. By carefully constraining the state variables, NMPC can enforce local geofencing to prevent the UAV from entering regions of potential entanglement, such as near masts, antennas, or parts of the USV superstructure. At the same time, it can guarantee the maximum tether length is not exceeded and that the interaction force between the UAV and LARS is maintained within safe operational limits. In the prior research [1], [2], it was demonstrated that the tether interaction force can be observed in the UAV's existing onboard sensors. Building on this concept, the state estimation based on UAV proprietary sensing and LARS encoder measurements is proposed. It will be further shown how estimation accuracy can be enhanced through active control of the tether interaction force. Finally, the proposed algorithms are implemented and experimentally verified on the custom LARS developed within the SeaClear project.

2.1 Modelling of tethered UAV

In this work, the variable tether length scenario is considered. Specifically, on the LARS, a tether management system is present, equipped with a cylinder-shaped actuator whose rotational motion leads to the variation in the tether length. An inertial coordinate frame $\{i\}$, aircraft fixed coordinate frame $\{a\}$ assumed to be attached to the centre of gravity, and a LARS fixed coordinate system $\{c\}$ are defined. The system, mounted on an USV, is illustrated in Fig. 3. Orientation of the aircraft frame relative to the inertial frame is described by the rotation matrix $\mathbf{R}_a^i$, obtained according to Z-Y-X convention:

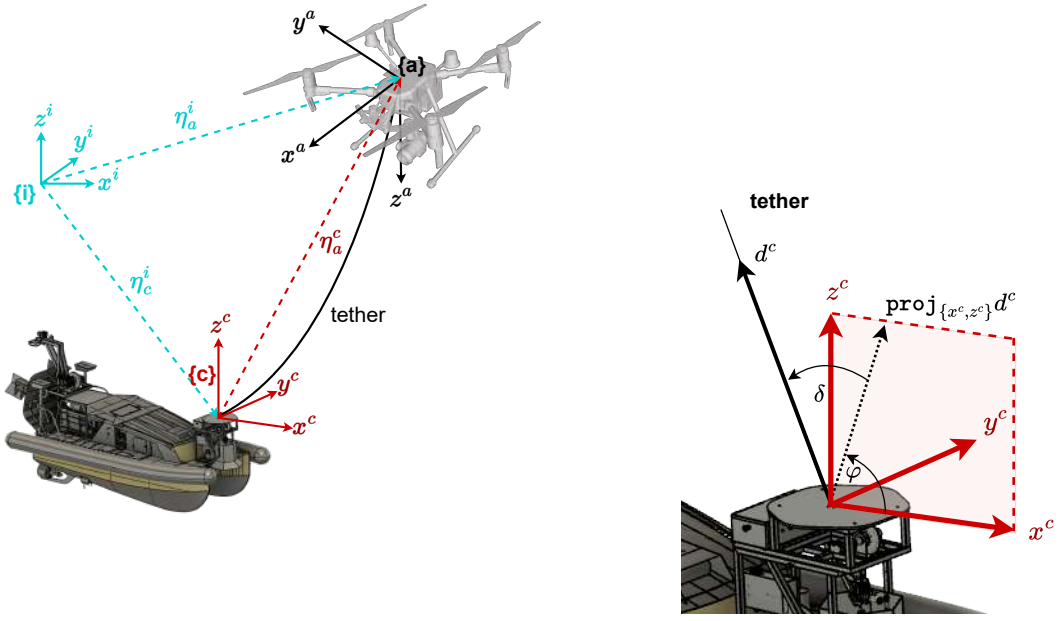
$$\mathbf{R}_a^i = \mathbf{R}_{z,\psi}\mathbf{R}_{y,\theta}\mathbf{R}_{x,\phi},$$

Co-funded by the European Union

SeaClear2.0 is co-funded by the European Union under the Horizon Europe Programme (Grant Agreement 101093822). Views and opinions expressed herein are those of the author(s) and do not necessarily reflect those of the European Union or European Climate, Infrastructure and Environment Executive Agency (CINEA). Neither the European Union nor the granting authority can be held responsible for them



Figure 2: Unmanned Aerial Vehicle (UAV) Launch and Recovery System (LARS) installed onboard the SeaCat Unmanned Surface Vehicle (USV) during SeaClear project demonstrations.



(a) (b)

Figure 3: a) Coordinate system representation for the unmanned aerial vehicle (UAV) tethered to a launch and recovery system (LARS), mounted on an unmanned surface vehicle (USV): Inertial coordinate frame is denoted $\{i\}$. The aircraft coordinate frame is denoted $\{a\}$ and fixed to the aircraft's centre of gravity. The LARS coordinate frame is denoted $\{c\}$. b) LARS coordinate system and tether angles definition. Elevation angle φ is the angle between the projection of d^c on $\{x^c, z^c\}$ plane and x^c. Azimuth angle δ is the angle between d^c and the plane $\{x^c, z^c\}$

Co-funded by the European Union

SeaClear2.0 is co-funded by the European Union under the Horizon Europe Programme (Grant Agreement 101093822). Views and opinions expressed herein are those of the author(s) and do not necessarily reflect those of the European Union or European Climate, Infrastructure and Environment Executive Agency (CINEA). Neither the European Union nor the granting authority can be held responsible for them

where ϕ, θ and ψ represent Euler angles *roll*, *pitch* and *yaw* respectively, and $\mathbf{R}_{z,\psi}\mathbf{R}_{y,\theta}\mathbf{R}_{x,\phi}$ are three principal rotations matrices

$$\mathbf{R}_{x,\phi} = \begin{bmatrix} 1 & 0 & 0 \\ 0 & \cos(\phi) & -\sin(\phi) \\ 0 & \sin(\phi) & \cos(\phi) \end{bmatrix}, \mathbf{R}_{y,\theta} = \begin{bmatrix} \cos(\theta) & 0 & \sin(\theta) \\ 0 & 1 & 0 \\ -\sin(\theta) & 0 & \cos(\theta) \end{bmatrix}, \mathbf{R}_{z,\psi} = \begin{bmatrix} \cos(\psi) & -\sin(\psi) & 0 \\ \sin(\psi) & \cos(\psi) & 0 \\ 0 & 0 & 1 \end{bmatrix}.$$

Note the mismatch of the *z* axis orientation in the $\{i\}$ and $\{a\}$ frame, outlined in Fig. 3.

Therefore, additional fixed transformation $\mathbf{R}_T$ is performed

$$\mathbf{R}_a^i = \mathbf{R}_T \mathbf{R}_a^i,$$

where

$$\mathbf{R}_T = \begin{bmatrix} 1 & 0 & 0 \\ 0 & -1 & 0 \\ 0 & 0 & -1 \end{bmatrix}.$$

As defined, $\mathbf{R}_a^i$ transforms vector in the $\{a\}$ frame, to $\{i\}$ frame, that is

$$v^i = \mathbf{R}_a^i v^a.$$

The association of Euler rates to aircraft angular velocity is defined as

$$\dot{\xi}_a = \mathbf{T}\omega_a^a, \tag{1}$$

where

$$\mathbf{T} = \begin{bmatrix} 1 & \sin(\phi)\tan(\theta) & \cos(\phi)\tan(\theta) \\ 0 & \cos(\phi) & -\sin(\phi) \\ 0 & \frac{\sin(\phi)}{\cos(\theta)} & \frac{\cos(\phi)}{\cos(\theta)} \end{bmatrix}.$$

In a similar fashion, this time without additional $\mathbf{R}_T$ transformation, the LARS orientation is given by $\mathbf{R}_c^i$.

Components of the tethered UAV system are related by the following vectors and parameters:
$\eta_a^i \in \mathbb{R}^{3\times1}$ - position of the origin of $\{a\}$ expressed in $\{i\}$,
$\eta_c^i \in \mathbb{R}^{3\times1}$ - position of the origin of $\{c\}$ expressed in $\{i\}$,
$\eta_a^c \in \mathbb{R}^{3\times1}$ - position of the origin of $\{a\}$ expressed in $\{c\}$,
$d^c \in \mathbb{S}^2$ - unit vector in the tether direction expressed in $\{c\}$,
$\xi_a \in \mathbb{R}^{3\times1}$ - vector of aircraft Euler angles,
$\xi_c \in \mathbb{R}^{3\times1}$ - vector of LARS Euler angles,
$\nu_a^a \in \mathbb{R}^{3\times1}$ - linear velocity of $\{a\}$ with respect to $\{i\}$ expressed in $\{a\}$,
$\nu_c^c \in \mathbb{R}^{3\times1}$ - linear velocity of $\{c\}$ with respect to $\{i\}$ expressed in $\{c\}$,
$\omega_a^a \in \mathbb{R}^{3\times1}$ - angular velocity of $\{a\}$ with respect to $\{i\}$ expressed in $\{a\}$,
$\omega_c^c \in \mathbb{R}^{3\times1}$ - angular velocity of $\{c\}$ with respect to $\{i\}$ expressed in $\{c\}$,
$\mathbf{\Omega}_c \in \mathbb{R}^{3\times3}$ - skew-symmetric matrix associated to ω_c^c,
$\theta_w \in \mathbb{R}$ - winch actuator angular position,

Co-funded by the European Union

SeaClear2.0 is co-funded by the European Union under the Horizon Europe Programme (Grant Agreement 101093822). Views and opinions expressed herein are those of the author(s) and do not necessarily reflect those of the European Union or European Climate, Infrastructure and Environment Executive Agency (CINEA). Neither the European Union nor the granting authority can be held responsible for them

$\tau_a \in \mathbb{R}^{3\times 1}$ - aircraft moment about its center of gravity expressed in $\{a\}$,
$\mathbf{I}_a \in \mathbb{R}^{3\times 3}$ - aircraft inertia matrix about its center of gravity,
$J_w \in \mathbb{R}^+$ - winch actuator inertia,
$r_w \in \mathbb{R}^+$ - winch actuator radius,
$m_a \in \mathbb{R}^+$ - aircraft mass,
$l \in \mathbb{R}_0^+$ - tether length,
$g \in \mathbb{R}^+$ - acceleration of gravity,
$F_t \in \mathbb{R}^+$ - magnitude of the aircraft thrust force,
$F_l \in \mathbb{R}_0^+$ - magnitude of the tether tension force,
$\tau_w \in \mathbb{R}$ - winch actuator input torque.

To simplify the system model, the following assumptions are introduced, deviating from the most general case:

Assumption 1 - *The tether attachment point is in the aircraft frame origin. Therefore, aircraft rotational dynamics are unaffected by the tether tension force.*

Assumption 2 - *Aircraft design is symmetric. Therefore, the aircraft inertia matrix $\mathbf{I}^a$ is diagonal.*

Assumption 3 - *LARS is considered to be an independent sub-system unaffected by the aircraft dynamics, with states available as measurements at all times. It supports both translational and rotational motion, as when mounted on an USV.*

Now, following the work in [3], the unit vector d^c in the tether direction is defined. Under the taut tether assumption, this will allow aircraft position to be expressed relative to the LARS as η_a^c. The unit vector d^c is parameterized by the elevation angle, $\varphi \in [0, 2\pi]$, and the azimuth angle, $\delta \in \left[-\frac{\pi}{2}, \frac{\pi}{2}\right]$, as

$$d^c = \begin{bmatrix} \cos(\delta)\cos(\varphi) \\ -\sin(\delta) \\ \cos(\delta)\sin(\varphi) \end{bmatrix}. \tag{2}$$

The azimuth angle δ is defined as the angle between d^c and the plane $\{x^c, z^c\}$, and the elevation angle φ as the angle between projection of d^c on $\{x^c, z^c\}$ and x^c, as depict in Fig. 3. b).

Therefore, the position of the aircraft in $\{c\}$ is

$$\eta_a^c = d^c l,$$

and in $\{i\}$, accordingly

$$\eta_a^i = \eta_c^i + \mathbf{R}_c^i d^c l. \tag{3}$$

The aircraft's linear velocity in the inertial frame is obtained by the differentiation of the previous equation

$$\dot{\eta}_a^i = \mathbf{R}_c^i \left(\nu_c^c + l\boldsymbol{\Omega}_c d^c + \dot{l}d^c + l\dot{d}^c\right). \tag{4}$$

Note that relation $\dot{\eta}_c^i = \mathbf{R}_c^i \nu_c^c$ is exploited. The aircraft inertial acceleration is obtained by additional differentiation of (4), leading to

Co-funded by the European Union

SeaClear2.0 is co-funded by the European Union under the Horizon Europe Programme (Grant Agreement 101093822). Views and opinions expressed herein are those of the author(s) and do not necessarily reflect those of the European Union or European Climate, Infrastructure and Environment Executive Agency (CINEA). Neither the European Union nor the granting authority can be held responsible for them

$$\ddot{\eta}_a^i = \mathbf{R}_c^i \left[\mathbf{\Omega}_c \left(\nu_c^c + l\mathbf{\Omega}_c d^c + 2\dot{l}d^c + 2l\dot{d}^c \right) + \dot{\nu}_c^c + l\dot{\mathbf{\Omega}}_c d^c + 2\dot{l}\dot{d}^c + \ddot{l}d^c + l\ddot{d}^c \right]. \tag{5}$$

Finally, the variables $q \in \mathbb{R}^{3\times 1}$ and $\mathbf{J}_q \in \mathbb{R}^{3\times 3}$ are defined as

$$q = \begin{bmatrix} l \\ \varphi \\ \delta \end{bmatrix}, \ \mathbf{J}_q = \begin{bmatrix} \cos(\delta)\cos(\varphi) & -l\cos(\delta)\sin(\varphi) & -l\cos(\varphi)\sin(\delta) \\ -\sin(\delta) & 0 & -l\cos(\delta) \\ \cos(\delta)\sin(\varphi) & l\cos(\delta)\cos(\varphi) & -l\sin(\delta)\sin(\varphi) \end{bmatrix}, \tag{6}$$

and substituted into (5), resulting in

$$\ddot{\eta}_a^i = \mathbf{R}_c^i \left[\mathbf{\Omega}_c \left(\nu_c^c + l\mathbf{\Omega}_c d^c + 2\mathbf{J}_q \dot{q} \right) + \dot{\nu}_c^c + l\dot{\mathbf{\Omega}}_c d^c + \dot{\mathbf{J}}_q \dot{q} + \mathbf{J}_q \ddot{q} \right].$$

To shorten this lengthy expression, a new variable a_c is introduced

$$a_c = \mathbf{\Omega}_c \left(\nu_c^c + l\mathbf{\Omega}_c d^c + 2\mathbf{J}_q \dot{q} \right) + \dot{\nu}_c^c + l\dot{\mathbf{\Omega}}_c d^c + \dot{\mathbf{J}}_q \dot{q},$$

leading to

$$\ddot{\eta}_a^i = \mathbf{R}_c^i \left(a_c + J_q \ddot{q} \right). \tag{7}$$

2.1.1 Newton-Euler equations

The aircraft under consideration is a unidirectional-thrust vehicle, meaning that thrust force is produced only in the $-z_a$ direction of the aircraft fixed coordinate frame. A general aircraft motion through space is then achieved by directing the thrust via a change of vehicle orientation.

For the given system, the translational dynamics of the aircraft in the inertial frame are as follows

$$m_a \ddot{\eta}_a^i = -\mathbf{R}_a^i \begin{bmatrix} 0 \\ 0 \\ F_t \end{bmatrix} - \begin{bmatrix} 0 \\ 0 \\ m_a g \end{bmatrix} - F_l \mathbf{R}_c^i d^c. \tag{8}$$

Under the declared assumptions, aircraft rotational dynamics are

$$\mathbf{I}_a \dot{\omega}_a^a = \mathbf{I}_a \omega_a^a \times \omega_a^a + \tau_a. \tag{9}$$

As stated, the case where the tether management system is available is considered. This system is composed of a rotational actuator (motor) coupled with a cylinder. When the motor applies an input torque, the tether is wound or unwound on the cylinder, depending on the direction of the applied torque. Under the mild assumption that changes in actuator inertia and radius are negligible, the tether actuator dynamics is

$$J_w \ddot{\theta}_w = \tau_w + F_l r_w.$$

Moreover, using the identity $l = r_w \theta_w$, the dynamics of the tether length are obtained

$$\frac{J_w}{r_w} \ddot{l} = \tau_w + F_l r_w. \tag{10}$$

Co-funded by the European Union

SeaClear2.0 is co-funded by the European Union under the Horizon Europe Programme (Grant Agreement 101093822). Views and opinions expressed herein are those of the author(s) and do not necessarily reflect those of the European Union or European Climate, Infrastructure and Environment Executive Agency (CINEA). Neither the European Union nor the granting authority can be held responsible for them

In the scope of this work, the aim is to estimate and control the relative position of the aircraft with respect to the LARS. This relative position is captured in (6), and characterized by the tether length, azimuth, and elevation angles. Thus, the dynamics of this variable are derived next.
To start, (7) is substituted into (8), which, after some rearrangements, results in

$$m_a \mathbf{J}_q \ddot{q} + F_l d^c = -f_c - f_t - f_g, \tag{11}$$

where elements

$$f_c = m_a a_c, \quad f_t = \mathbf{R}_i^c \mathbf{R}_a^i \begin{bmatrix} 0 \\ 0 \\ F_t \end{bmatrix}, \quad f_g = \mathbf{R}_i^c \begin{bmatrix} 0 \\ 0 \\ m_a g \end{bmatrix},$$

are introduced to shorten the notation. By combining (11) and (10), a subsequent system is formed

$$\begin{bmatrix} m_a \mathbf{J}_q & d^c \\ \begin{bmatrix} \frac{J_w}{r_w} & 0 & 0 \end{bmatrix} & -r_w \end{bmatrix} \begin{bmatrix} \ddot{q} \\ F_l \end{bmatrix} = \begin{bmatrix} -f_c - f_t - f_g \\ \tau_w \end{bmatrix}.$$

Here, for brevity, a matrix $\mathbf{M} \in \mathbb{R}^{4\times4}$ is defined as

$$\mathbf{M} = \begin{bmatrix} m_a \mathbf{J}_q & d^c \\ \begin{bmatrix} \frac{J_w}{r_w} & 0 & 0 \end{bmatrix} & -r_w \end{bmatrix}.$$

It is important to mention the singularity of the matrix at $l = 0$ or $|\delta| = \frac{\pi}{2}$. However, this is merely a theoretical concern, as in practice, it is unlikely for the system to reach that state. Considering this, the complete system dynamics are finally given as

$$\ddot{q} = \begin{bmatrix} \mathbf{I}^{3\times3} & 0^{3\times1} \end{bmatrix} \mathbf{M}^{-1} \begin{bmatrix} -f_c - f_t - f_g \\ \tau_w \end{bmatrix}, \tag{12}$$

$$F_l = \begin{bmatrix} 0^{1\times3} & 1 \end{bmatrix} \mathbf{M}^{-1} \begin{bmatrix} -f_c - f_t - f_g \\ \tau_w \end{bmatrix},$$

where $\mathbf{I}^{3\times3}$, $0^{3\times1}$ and $0^{1\times3}$ are the identity matrix and zero vectors.

2.2 Nonlinear Model Predictive Controller

In this subsection, a Nonlinear Model Predictive Controller for UAV trajectory tracking and tether interaction force control is described.

2.2.1 Plant model

The plant state vector $x \in \mathbb{R}^{12\times1}$, control input vector $u \in \mathbb{R}^{5\times1}$, vector of LARS states $d \in \mathbb{R}^{15\times1}$ regarded as the vector of measured disturbances, and output vector $y \in \mathbb{R}^{12\times1}$ are respectively defined

Co-funded by the European Union

SeaClear2.0 is co-funded by the European Union under the Horizon Europe Programme (Grant Agreement 101093822). Views and opinions expressed herein are those of the author(s) and do not necessarily reflect those of the European Union or European Climate, Infrastructure and Environment Executive Agency (CINEA). Neither the European Union nor the granting authority can be held responsible for them

as

$$
\begin{aligned}
x &= \begin{bmatrix} q & \dot{q} & \xi_a & \omega_a^a \end{bmatrix}^T, \\
u &= \begin{bmatrix} \tau_w & F_t & \tau_a \end{bmatrix}^T, \\
d &= \begin{bmatrix} \nu_c^c & \dot{\nu}_c^c & \xi_c & \omega_c^c & \dot{\omega}_c^c \end{bmatrix}^T, \\
y &= \mathbf{I}x,
\end{aligned}
$$

where $\mathbf{I} \in \mathbb{R}^{12\times 12}$ is the identity matrix. Hence, the nonlinear plant model is

$$
\begin{aligned}
\dot{x} &= f\left(x, u, d\right), \\
\dot{x} &= \begin{bmatrix} \dot{q} & \ddot{q} & \dot{\xi}_a & \dot{\omega}_a^a \end{bmatrix}^T,
\end{aligned}
\tag{13}
$$

where $\ddot{q}, \dot{\xi}_a$ and $\dot{\omega}_a^a$ are stated in (12), (1), (9), respectively.

2.2.2 Controller formulation

Nonlinear Model Predictive Controller, at each control interval k, calculates control action over the prediction horizon $p \in \mathbb{R}_0^+$, that minimizes cost function J_k while satisfying input and state constraints. Only the first control input is then applied to the system, and the process is repeated in a receding horizon manner. This optimization problem is a nonlinear program, defined as

$$
\begin{aligned}
J_k^*\left(x_k, u_k\right) \min_{\mathrm{U}} & \sum_{i=0}^{p-1} \Big[\left(e_{y_{k+i}}^T \mathbf{Q} e_{y_{k+i}} \right) + \left(e_{u_{k+i}}^T \mathbf{R}_u e_{u_{k+i}} \right) \\
& \qquad + \left(\Delta u_{k+i}^T \mathbf{R}_{\Delta u} \Delta u_{k+i} \right) \Big] + \rho_\epsilon \epsilon_k^2 \\
\text{subject to} \quad & x_{k+i+1} = f_d\left(x_{k+i}, u_{k+i}, d_k\right) \\
& x_{k+i} \in \mathcal{X} \\
& u_{k+i} \in \mathcal{U} \\
& x_0 = x\left(0\right)
\end{aligned}
\tag{14}
$$

where

$$
\begin{aligned}
\mathrm{U} &= \begin{bmatrix} u_k & u_{k+1} & \dots & u_{k+p-1} & \epsilon_k \end{bmatrix}, \\
e_{y_{k+i}} &= \left(y_{r_{k+i+1}} - y_{k+i+1} \right), \\
e_{u_{k+i}} &= \left(u_{r_{k+i}} - u_{k+i} \right), \\
\Delta u_{k+i} &= \left(u_{k+i} - u_{k+i-1} \right).
\end{aligned}
$$

The remaining variables are listed below
$J_k^* \in \mathbb{R}_0^+$ - cost function value at time interval k,
$\mathrm{U} \in \mathbb{R}^{5\times p}$ - optimized control action over the prediction horizon,
$i \in \mathbb{R}^+$ - prediction horizon step,

Co-funded by the European Union

SeaClear2.0 is co-funded by the European Union under the Horizon Europe Programme (Grant Agreement 101093822). Views and opinions expressed herein are those of the author(s) and do not necessarily reflect those of the European Union or European Climate, Infrastructure and Environment Executive Agency (CINEA). Neither the European Union nor the granting authority can be held responsible for them

$\epsilon_k \in \mathbb{R}_0^+$ - constraint violation slack variable at time interval k,
$\rho_\epsilon \in \mathbb{R}_0^+$ - constraint violation penalty weight,
$\mathbf{Q} \in \mathbb{R}^{12\times12} \mid \mathbf{Q} \succeq 0$ - output penalty weight matrix,
$\mathbf{R}_u \in \mathbb{R}^{5\times5} \mid \mathbf{R}_u \succeq 0$ - input penalty weight matrix,
$\mathbf{R}_{\Delta u} \in \mathbb{R}^{5\times5} \mid \mathbf{R}_{\Delta u} \succeq 0$ - input rate penalty weight matrix,
$\mathcal{X} \in \mathbb{R}^{12\times1}$ - set of the state constraints,
$\mathcal{U} \in \mathbb{R}^{5\times1}$ - set of the input constraints,
$f_d\left(x_{k+i}, u_{k+i}, d_k\right) \in \mathbb{R}^{12\times1}$ - discretized plant model,
$y_{k+i} \in \mathbb{R}^{12\times1}$ - predicted plant output at the i-th prediction horizon step,
$y_{r_{k+i}} \in \mathbb{R}^{12\times1}$ - output reference value at the i-th prediction horizon step,
$u_{r_{k+i}} \in \mathbb{R}^{5\times1}$ - input reference value at the i-th prediction horizon step,
$e_{y_{k+i}} \in \mathbb{R}^{12\times1}$ - predicted output tracking error at the i-th prediction horizon step,
$e_{u_{k+i}} \in \mathbb{R}^{5\times1}$ - predicted input tracking error at the i-th prediction horizon step,
$\Delta u_{k+i} \in \mathbb{R}^{5\times1}$ - input change between i-th and $(i-1)$-th prediction horizon step.

If both the input and the output constraints are set as hard constraints, meaning they must be met in the optimization problem, solving the optimization problem could become infeasible. In that case, some of the constraints can be designated as soft, meaning that the controller can deem a solution U optimal, despite the constraint violation. The constraint softening is achieved by introducing a slack variable ϵ_k for constraint violation as

$$x_{min} - \epsilon_k x_{min} \leq x_{k+i} \leq x_{max} + \epsilon_k x_{max},$$

where x_{min} and x_{max} are the state lower and upper bound. When the optimization problem is feasible, equivalence is achieved through the appropriate selection of the constraint violation penalty weight. As highlighted earlier, the LARS is treated as an independent system with available measurements but without a known model. Therefore, it is not possible to preview the measured disturbances, and they are assumed to remain constant throughout the prediction horizon, as indicated in (14).

2.2.3 Controller implementation

The aforementioned controller is implemented in Matlab®Simulink with the Model Predictive Control Toolbox [4]. To start, the continuous-time prediction model is defined as (13). Subsequently, the discretization of this model, achieved through the implicit trapezoidal rule, yields the discrete plant model f_d. A performance comparison with the Euler and fourth-order Runge-Kutta methods showed similar accuracy, with the latter having slower execution times, making the trapezoidal method the preferred option. At this point, the output vector is presumed to be available, and the matter of state estimation is addressed in the following section.

With five available inputs, it is possible to control either five outputs or inputs to track the desired trajectories. The selection is encoded in the weight matrices

$$\begin{aligned}\mathbf{Q} &= (w_{y_1}^2, \ldots, w_{y_{12}}^2),\\ \mathbf{R}_u &= (w_{u_1}^2, \ldots, w_{u_5}^2),\\ \mathbf{R}_{\Delta u} &= (w_{\Delta u_1}^2, \ldots, w_{\Delta u_5}^2),\end{aligned}$$

with input and output weights, specified in Table 1. From the output weights, it is evident that control

Co-funded by the European Union

SeaClear2.0 is co-funded by the European Union under the Horizon Europe Programme (Grant Agreement 101093822). Views and opinions expressed herein are those of the author(s) and do not necessarily reflect those of the European Union or European Climate, Infrastructure and Environment Executive Agency (CINEA). Neither the European Union nor the granting authority can be held responsible for them

Table 1: NMPC Weights and Constraints

Output parameters				
x	w_y	x_{min}	x_{max}	Unit
l	5	0.1	50	m
φ	5	0	2π	rad
δ	5	$-\frac{\pi}{2}$	$\frac{\pi}{2}$	rad
$\dot{l}$	0	-1.5	1.5	$\mathrm{m\,s^{-1}}$
$\dot{\varphi}$	0	$-\infty$	∞	$\mathrm{rad\,s^{-1}}$
$\dot{\delta}$	0	$-\infty$	∞	$\mathrm{rad\,s^{-1}}$
ϕ	0	$-\frac{\pi}{6}$	$\frac{\pi}{6}$	rad
θ	0	$-\frac{\pi}{6}$	$\frac{\pi}{6}$	rad
ψ	1	$-\pi$	π	rad
$\omega^a_{a_x}$	0	$-\frac{5\pi}{3}$	$\frac{5\pi}{3}$	$\mathrm{rad\,s^{-1}}$
$\omega^a_{a_y}$	0	$-\frac{5\pi}{3}$	$\frac{5\pi}{3}$	$\mathrm{rad\,s^{-1}}$
$\omega^a_{a_z}$	0	$-\frac{3\pi}{5}$	$\frac{3\pi}{5}$	$\mathrm{rad\,s^{-1}}$
Input parameters				
u	w_u	u_{min}	u_{max}	Unit
τ_w	10	-1.5	-0.15	N m
F_t	0	0	90	N
τ_{a_x}	0	-10	10	N m
τ_{a_y}	0	-10	10	N m
τ_{a_z}	0	-10	10	N m

is applied to the UAV yaw angle ψ, and its relative position with respect to the LARS, i.e., q. This choice leaves one input unused, τ_w, which is utilized to control the tether tension force F_l. Specifically, given a reference tension force F_{l_r}, equation (10) is solved for τ_w. Since the $\ddot{l}$ is not readily available, $\dot{l}$ is filtered by a low-pass filter and differentiated to calculate the control input reference. Beyond the evident safety considerations, the control of the tension force enables additional operational flexibility. For instance, in scenarios where power consumption is a priority, non-taut tether management strategies, such as those based on catenary tether modelling, can be implemented. In contrast, for the taut-tether strategies, tether tension control can provide additional robustness to outside disturbances, it can be employed for improved state estimation. Finally, aggressive control actions are penalized by setting the input rate weight $w_{\Delta u} = 0.1$, for all inputs.

Physical limitations of the system are represented by a set of state and input constraints

$$\mathcal{X} = \left\{ x \in \mathbb{R}^{12\times 1} | x_{min} < x < x_{max} \right\},$$
$$\mathcal{U} = \left\{ u \in \mathbb{R}^{5\times 1} | u_{min} < u < u_{max} \right\},$$

each with minimum x_{min}, and maximum x_{max} value, as outlined in the Table 1. Constraints are predicated on the DJI Matrice 210v2 Real-Time Kinematics (RTK) [5], UAV model employed in both simulations

Co-funded by the European Union

SeaClear2.0 is co-funded by the European Union under the Horizon Europe Programme (Grant Agreement 101093822). Views and opinions expressed herein are those of the author(s) and do not necessarily reflect those of the European Union or European Climate, Infrastructure and Environment Executive Agency (CINEA). Neither the European Union nor the granting authority can be held responsible for them

and experimental validation. Input constraints for τ_w are determined from (10), at steady state $\ddot{l} = 0$, for the desired maximum and minimum tension force values.

With the input and output references, measurements, weight matrices, and constraints in place, the Sequential Quadratic Programming (SQP) algorithm is employed to solve the optimization problem (14).

2.3 Simulations

The numerical simulations are performed in Matlab®Simulink. With no available prediction model for the measured disturbances, it is not efficient to compute control actions over the entire prediction horizon. Preferably, control actions are optimized for a segment of the prediction horizon, and for the remainder control remains constant. The parameter that specifies the number of time steps within the prediction horizon, over which control actions are calculated is the control horizon.

In the simulation scenario, the LARS is mounted on a USV which navigates under the influence of waves. The presence of waves is emulated by oscillating roll, pitch, yaw, and heave motion. Its states are generated in Simulink and assumed to be measured disturbances for the NMPC. Simultaneously, the UAV is tasked with tracking the reference trajectory relative to the LARS, while the tether tension force is controlled through τ_w. Tracking results for both the UAV and LARS East-North-Up (ENU) positions, alongside the reference trajectory transformed into the ENU frame, are outlined in Fig. 5.

Presented results indicate the capability of the controller to cope with the unpredictable USV motion and waves, while satisfying the input and output constraints, therefore validating the viability of the proposed control approach.

2.4 Experimental Setup and Implementation Details

For the experimental validation of the proposed algorithms, it is essential to consider several key factors. These include system parameter uncertainties, the need for real-time execution, and the constraints imposed by the existing low-level control structures on the experimental platform. The following subsections will introduce the experimental platform and provide implementation details of the control and estimation algorithms, ensuring that they align with these considerations.

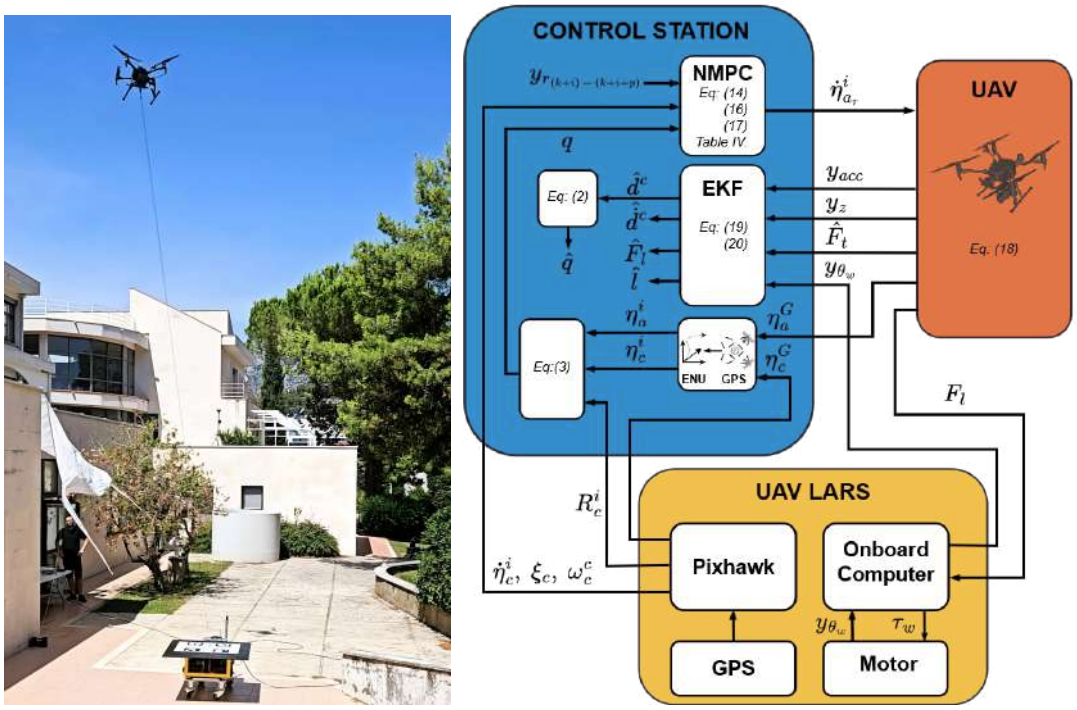
Experimental platform The experimental platform consists of three primary components: the UAV, the LARS, and the Ground Control Station (GCS). An image of the experimental platform captured during the experimental verification is shown in Fig. 4.

UAV The aerial platform used for experimental validation is the DJI Matrice 210v2 RTK. This UAV is equipped with a Manifold 2G onboard computer running Ubuntu 16.04 and Robot Operating System (ROS) Kinetic. The DJI Onboard SDK [6] software package provides access to the aircraft's sensor data and integrated controllers, which include position, velocity, and attitude control. In addition to the onboard sensor suite, a load cell sensor is installed to provide cable tension measurements.

LARS The main element of the LARS is the Brushless Direct Current (BLDC) actuator. This motor features an integrated controller with position, velocity, and torque operating modes. It utilizes a magnetic multi-turn absolute encoder for position and velocity feedback, offering a 17-bit single-turn and 16-bit multi-

Co-funded by the European Union

SeaClear2.0 is co-funded by the European Union under the Horizon Europe Programme (Grant Agreement 101093822). Views and opinions expressed herein are those of the author(s) and do not necessarily reflect those of the European Union or European Climate, Infrastructure and Environment Executive Agency (CINEA). Neither the European Union nor the granting authority can be held responsible for them



(a) (b)

Figure 4: a) Overview of the experimental platform. The LARS is located at the bottom centre of the image, while the tethered UAV is at the top left. The image was captured during the experimental verification at the Laboratory for Intelligent Autonomous Systems (LARIAT), University of Dubrovnik. b) Overview of the experimental setup, highlighting the relevant signals and the distribution of the proposed control and estimation algorithms across the experimental platforms. The Control station processes measurements from both the UAV and the UAV LARS, executing the NMPC and EKF algorithms. The UAV receives trajectory tracking velocity references from the NMPC, while the UAV LARS regulates the tether tension.

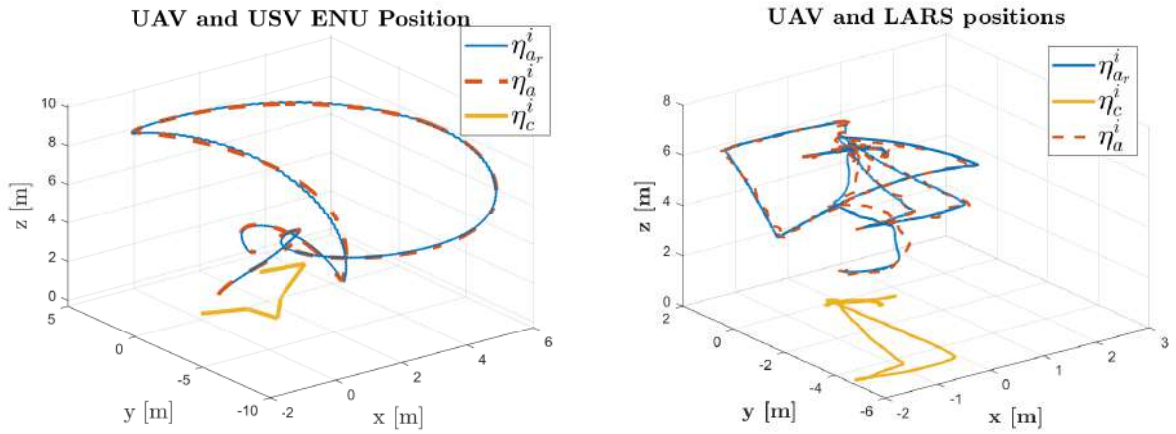
turn encoder resolution. The motor shaft is coupled to the cable reel, which houses the UAV tether. The motor is interfaced with the rest of the system via the LARS onboard computer. The LARS position and attitude measurements are provided by Pixhawk Autopilot, which receives Global Positioning System (GPS)-RTK input from the Emlid Reach M2 module.

GCS The Ground Control Station is the primary platform for implementing control and estimation algorithms, operating on Ubuntu 20.04 with ROS Noetic. The algorithms are developed in Matlab®Simulink. Data exchange between the GCS, LARS, and UAV is managed via the ROS network.

A comprehensive overview of the experimental setup and the implementation details of the proposed algorithms across the experimental platforms is depicted in Fig. 4. b).

Co-funded by the European Union

SeaClear2.0 is co-funded by the European Union under the Horizon Europe Programme (Grant Agreement 101093822). Views and opinions expressed herein are those of the author(s) and do not necessarily reflect those of the European Union or European Climate, Infrastructure and Environment Executive Agency (CINEA). Neither the European Union nor the granting authority can be held responsible for them



(a) (b)

Figure 5: a) Simulated UAV (red dashed) and LARS (yellow) positions in ENU world frame. Depicted reference trajectory (blue) represents q references transformed to ENU world frame. b) Output reference tracking results during experimental verification: output reference (blue) and ground truth outputs (red dashed). Both graphs show the LARS position (yellow), aircraft reference position (blue), and aircraft ground truth position (red dashed), given in the inertial reference frame during experimental verification.

2.4.1 Experimental validation

The experimental validation of the proposed control and estimation algorithms was conducted at the Laboratory for Intelligent Autonomous Systems (LARIAT), University of Dubrovnik. A series of experiments and subsequent analyses were performed to evaluate the effectiveness of these algorithms. The following section presents the results of one such experiment, with an available video [3].

During the experiment, the UAV was tasked with following a reference trajectory using a NMPC. The control loop was closed using feedback from GPS-RTK measurements, which were transformed into controller states based on the kinematic transformations. These GPS-RTK measurements also served as ground truth information for tracking and estimation validation. The tension force control loop is closed utilizing the load cell measurements. The NMPC output tracking performance, are presented in Fig. 5. To demonstrate the controller's robustness against various measured disturbances, the LARS underwent a range of translational and attitude motions.

The results demonstrate that the proposed NMPC can successfully track a given trajectory and effectively respond to measured disturbances. Except for a temporary loss of the GPS-RTK fix at the beginning of the experiment, tracking errors in azimuth and elevation angles did not exceed $0.0715\,\mathrm{rad}$ (4.1 degrees). The maximum length tracking error is $15\,\mathrm{cm}$. The poorest tracking performance was observed in the tension force control, attributed to the narrow operating torque window of the actuator. This can be mitigated in the future by selecting a more suitable actuator and integrating the tension control into the NMPC structure.

The comparison between the estimates and ground truth data validates the proposed estimation work-

[3] Experimental validation video - https://youtu.be/0qUJN51v54c

Co-funded by the European Union

SeaClear2.0 is co-funded by the European Union under the Horizon Europe Programme (Grant Agreement 101093822). Views and opinions expressed herein are those of the author(s) and do not necessarily reflect those of the European Union or European Climate, Infrastructure and Environment Executive Agency (CINEA). Neither the European Union nor the granting authority can be held responsible for them

flow with minimal proprietary onboard sensing. Elevation and azimuth angle RMSE is $0.1\,\mathrm{rad}$ (5.7 degrees). The observed reduction in estimation error with increasing reference tension force, supports the utilization of tension force control in enhancing estimation accuracy.

2.5 Conclusion

In this section, a cooperative control framework for a tethered UAV system based on the Nonlinear Model Predictive Control (NMPC) method was presented. The effectiveness of the proposed control method was validated through a series of experiments, where the UAV demonstrated accurate tracking of user-defined trajectories in the presence of external disturbances. The experimental results also highlighted how minimal proprietary sensing can be employed to estimate the UAV's relative position, even in scenarios involving translational and rotational LARS movements. It was further demonstrated that active interaction force control can enhance the estimation accuracy. The proposed framework will be assessed in the upcoming SeaClear2.0 project trials, where the UAV-LARS system will be deployed from an autonomous unmanned surface vehicle (USV) in a real-world operating environment. More details on the work done on this topic within SeaClear and SeaClear 2.0 project can be found in publications [1], [2], [7], [8]

Co-funded by the European Union

SeaClear2.0 is co-funded by the European Union under the Horizon Europe Programme (Grant Agreement 101093822). Views and opinions expressed herein are those of the author(s) and do not necessarily reflect those of the European Union or European Climate, Infrastructure and Environment Executive Agency (CINEA). Neither the European Union nor the granting authority can be held responsible for them

3 USV control upgrade

3.1 SeaCat control

In this section, we report on the update to the SeaCat2.0 control system USV. In particular, the focus is on the Dynamic Positioning (DP) (sometimes also called station keeping) control algorithm of the SeaCat2.0 USV. With respect to the SeaCat USV that was part of SeaClear, the SeaCat2.0 USV has additional bow thrusters that increase its capabilities in terms of DP control.

In the remainder of this section we first introduce a dynamical model of the SeaCat2.0 USV (in Section 3.1.1). The model enables the development of a model-based controller, which will be one of the main future directions of work about the SeaCat2.0 USV control. In addition, following an approach similar to that used in SeaClear, we design a Proportional-Integral-Derivative (PID) controller to use as a baseline for the tests that will be conducted on the dynamic positioning controllers (Section 3.1.2).

3.1.1 Modelling of the SeaCat2.0

We start by introducing a set of reference frames commonly used in maneuvering theory for marine crafts [9]. The relevant reference frames are represented in Figure 6.

- $\{e\} = (O^{\mathrm{e}}, x^{\mathrm{e}}, y^{\mathrm{e}})$ is an earth-fixed inertial reference frame. The standard orientation adopted is that having the x axis pointing North and the y axis pointing East;
- $\{b\} = (O^{\mathrm{b}}, x^{\mathrm{b}}, y^{\mathrm{b}})$ is a body-fixed reference frame. The x axis, while the y axis points toward the starboard side of the craft;
- $\{r\} = (O^{\mathrm{r}}, x^{\mathrm{r}}, y^{\mathrm{r}})$ is the target reference frame. The orientation ψ^{r} is the desired heading for the boat. In maneuvering theory, it is common to assume that the desired heading changes slowly over time, i.e., $\dot{\psi}^{\mathrm{r}} \approx 0$;
- $\{p\} = (O^{\mathrm{p}}, x^{\mathrm{p}}, y^{\mathrm{p}})$ is the reference-parallel reference frame. Its origin coincides with that of $\{b\}$, i.e., $O^{\mathrm{p}} \equiv O^{\mathrm{b}}$, while the orientation is the same of $\{r\}$, i.e., $\psi^{\mathrm{p}} \equiv \psi^{\mathrm{r}}$. When close enough to $\{r\}$, the reference-parallel reference frame can be used to linearize the model.

Given the reference frames listed above, we introduce a point-mass nonlinear dynamical model in the i.e., horizontal plane. Following the convention used for the dynamical modelling of USVs for the purpose of DP, we only consider three Degrees of Freedoms (DOFs), namely, surge, sway, and yaw [9]. The nonlinear 3 DOF model is given by:

$$\begin{aligned} \boldsymbol{M}\dot{\boldsymbol{\nu}} + \boldsymbol{C}(\boldsymbol{\nu})\boldsymbol{\nu} + \boldsymbol{D}_{\mathrm{L}}\boldsymbol{\nu} + \boldsymbol{D}_{\mathrm{NL}}(\boldsymbol{\nu})\boldsymbol{\nu} &= \boldsymbol{b} + \boldsymbol{\tau}_{\mathrm{control}} \\ \dot{\boldsymbol{\eta}} &= \boldsymbol{R}(\psi)\boldsymbol{\nu} \end{aligned} \tag{15}$$

where:

- $\boldsymbol{\eta} = [x, y, \psi]^{\top}$ is the position of the USV expressed in $\{e\}$;

Co-funded by the European Union

SeaClear2.0 is co-funded by the European Union under the Horizon Europe Programme (Grant Agreement 101093822). Views and opinions expressed herein are those of the author(s) and do not necessarily reflect those of the European Union or European Climate, Infrastructure and Environment Executive Agency (CINEA). Neither the European Union nor the granting authority can be held responsible for them

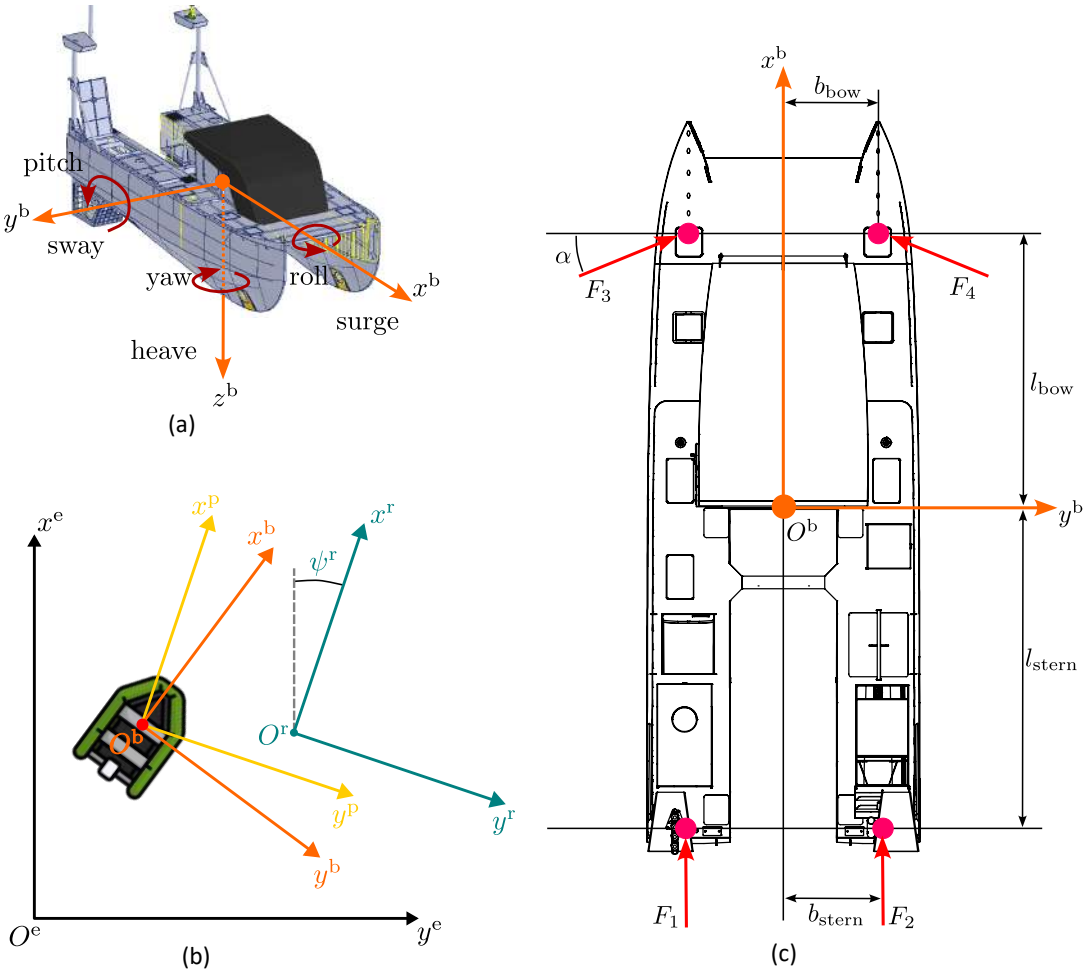


Figure 6: Reference frames used in the modeling of the SeaCAT2.0. In (a), the degrees of freedom of a marine craft. In (b), the relevant reference frames in the horizontal planes used in the modelling process. In (c), a top-view of the SeaCat2.0 USV with the main geometries and the thrusters.

- $\boldsymbol{\nu} = [u, v, r]^\top$ is the velocity of the USV expressed in $\{b\}$;
- $\boldsymbol{M}$ is the inertia matrix, which includes both the rigid-body and the added mass terms, i.e., $\boldsymbol{M} = \boldsymbol{M}_{\text{RB}} + \boldsymbol{M}_{\text{A}}$. The matrix $\boldsymbol{M}$ is then given by

$$\boldsymbol{M} = \begin{bmatrix} m & 0 & 0 \\ 0 & m & mx_g \\ 0 & mx_g & I_z \end{bmatrix} + \begin{bmatrix} X_{\dot{u}} & 0 & 0 \\ 0 & Y_{\dot{v}} & Y_{\dot{r}} \\ 0 & Y_{\dot{r}} & N_{\dot{r}} \end{bmatrix} = \begin{bmatrix} m + X_{\dot{u}} & 0 & 0 \\ 0 & m + Y_{\dot{v}} & mx_g + Y_{\dot{r}} \\ 0 & mx_g + Y_{\dot{r}} & I_z + N_{\dot{r}} \end{bmatrix}.$$

  $X_{\dot{u}}, Y_{\dot{v}}, N_{\dot{r}}, Y_{\dot{r}}$ are the hydrodynamic added masses, and x_g is the distance along x^{b} between O^{b} and the boat's center of mass;
- $\boldsymbol{C}(\boldsymbol{\nu})$ is the Coriolis centripetal matrix, which includes both the rigid-body and the added mass

Co-funded by the European Union

SeaClear2.0 is co-funded by the European Union under the Horizon Europe Programme (Grant Agreement 101093822). Views and opinions expressed herein are those of the author(s) and do not necessarily reflect those of the European Union or European Climate, Infrastructure and Environment Executive Agency (CINEA). Neither the European Union nor the granting authority can be held responsible for them

terms, i.e., $\boldsymbol{C}(\boldsymbol{\nu}) = \boldsymbol{C}_{\mathrm{RB}}(\boldsymbol{\nu}) + \boldsymbol{C}_{\mathrm{A}}(\boldsymbol{\nu})$. The matrix $\boldsymbol{C}(\boldsymbol{\nu})$ is then given by

$$\boldsymbol{C}(\boldsymbol{\nu}) = \begin{bmatrix} 0 & 0 & -m(x_g r + v) \\ 0 & 0 & mu \\ m(x_g r + v) & -mu & 0 \end{bmatrix} + \begin{bmatrix} 0 & 0 & -Y_{\dot{v}} v - Y_{\dot{r}} r \\ 0 & 0 & X_{\dot{u}} u \\ Y_{\dot{v}} v + Y_{\dot{r}} r & -X_{\dot{u}} u & 0 \end{bmatrix}$$
$$= \begin{bmatrix} 0 & 0 & -(m + Y_{\dot{v}})v - (mx_g + Y_{\dot{r}})r \\ 0 & 0 & (m + X_{\dot{u}})u \\ (m + Y_{\dot{v}})v + (mx_g + Y_{\dot{r}})r & -(m + X_{\dot{u}})u & 0 \end{bmatrix}.$$

- $\boldsymbol{D}_L$ is the linear damping matrix, which represents the most relevant damping term at low velocities, and is defined as

$$\boldsymbol{D}_{\mathrm{L}} = \begin{bmatrix} X_u & 0 & 0 \\ 0 & Y_v & Y_r \\ 0 & N_v & N_r \end{bmatrix}.$$

  The linear damping terms prevail over the nonlinear ones up to 2 m/s [9]. Under this speed, the damping effects can be approximated with the linear terms only. Above 2 m/s, the nonlinear damping term should be taken into account as well.

- $\boldsymbol{b}$ represents a bias vector that collects the drift effects of wind, waves, and ocean currents. For our application case it is reasonable to assume that the current bias vector $\boldsymbol{b}^{\mathrm{e}}$ (i.e., the bias vector expressed in the earth reference frame) is almost stationary, i.e., $\dot{\boldsymbol{b}}^{\mathrm{e}} \approx \boldsymbol{0}$. The vector $\boldsymbol{b}$ is then computed simply by rotating $\boldsymbol{b}^{\mathrm{e}}$ in the body reference frame. In dynamic positioning, we can assume that this vector is known via observation/estimation of the water current;

- $\boldsymbol{\tau}_{\mathrm{control}} = [\tau_{\mathrm{surge}}, \tau_{\mathrm{sway}}, \tau_{\mathrm{yaw}}]^\top$ is the control action applied to the center of mass of the USV.

The model defined in (15) is nonlinear. In order to obtain a linear model of the USV, the following assumptions and simplifications are introduced:

1. The USV operates at low speed ($\leq$ 2 m/s). Therefore, the Coriolis centripetal term and the nonlinear damping term can be ignored;
2. The current bias vector $\boldsymbol{b}$ is stationary, i.e., $\dot{\boldsymbol{b}} = 0$;
3. The heading error between the body-fixed reference frame $\{b\}$ and the reference-parallel frame $\{p\}$ is small. Therefore, the assumption of small angles holds, i.e., $\boldsymbol{R}(\psi) \approx \boldsymbol{I}$;
4. The off-diagonal terms in the matrices $\boldsymbol{M}$ and $\boldsymbol{D}_{\mathrm{L}}$ are ignored. This leads to a dynamic model where the motion along each degree of freedom is decoupled from the others.

Under these assumption, the following linear model is obtained:

$$\begin{aligned} \boldsymbol{M}\dot{\boldsymbol{\nu}} + \boldsymbol{D}_{\mathrm{L}}\boldsymbol{\nu} &= \boldsymbol{b} + \boldsymbol{\tau}_{\mathrm{control}} \\ \dot{\boldsymbol{\eta}} &= \boldsymbol{\nu} \end{aligned} \tag{16}$$

Co-funded by the European Union

SeaClear2.0 is co-funded by the European Union under the Horizon Europe Programme (Grant Agreement 101093822). Views and opinions expressed herein are those of the author(s) and do not necessarily reflect those of the European Union or European Climate, Infrastructure and Environment Executive Agency (CINEA). Neither the European Union nor the granting authority can be held responsible for them

where the vectors $\boldsymbol{\nu}$ and $\boldsymbol{b}$ are now expressed in $\{p\}$. All the parameters that appear in the SeaCat2.0 model have been estimated using geometric and CAD data available from project specification [9–12]. The refinement of the estimation of the parameters via real data will be carried out if deemed necessary in the experimental validation of the model. The parameters values are reported in Table 2.

In the dynamic models (15) and (16) the control input $\boldsymbol{\tau}_{\text{control}}$ is a vector of forces to be applied to the center of mass. To determine the control input vector $\boldsymbol{u} = [u_1, u_2, u_3, u_4]^\top$, a thrust allocation problem needs to be solved. To do so, a thrusters configuration matrix is defined from the geometries introduced in Figure 6(c), which satisfies the relation

$$\boldsymbol{\tau}_{\text{control}} = \boldsymbol{T}\boldsymbol{u}.$$

The thrusters configuration matrix is defined as

$$\boldsymbol{T} = \begin{bmatrix} 1 & 1 & \sin\alpha & \sin\alpha \\ 0 & 0 & \cos\alpha & -\cos\alpha \\ b_{\text{stern}} & -b_{\text{stern}} & l_{\text{bow}}\cos\alpha + b_{\text{bow}}\sin\alpha & -l_{\text{bow}}\cos\alpha - b_{\text{bow}}\sin\alpha \end{bmatrix}.$$

To find the control inputs to apply to the thrusters of the USV, the following thrust allocation problem is solved

$$\begin{aligned} &\min_{\boldsymbol{u}} \boldsymbol{u}^\top \boldsymbol{W}\boldsymbol{u} \\ &\text{s.t. } \boldsymbol{T}\boldsymbol{u} - \boldsymbol{\tau}_{\text{control}} = \boldsymbol{0}. \end{aligned} \tag{17}$$

where $\boldsymbol{W}$ is a diagonal weighting matrix. A closed-form solution to problem (17) exists so that the inverse relation can be obtained.

Finally, empirical observations during SeaClear have shown that there exists a delay between the input signal $\boldsymbol{u}$ provided to the thrusters and the actuation force $\boldsymbol{F} = [F_1, F_2, F_3, F_4]^\top$ generated by the thrusters. As a first approximation, this delay is modeled with a 1st-order low-pass filter as

$$\dot{F}_i = \frac{u_i - F_i}{T_i}, \tag{18}$$

where the time constant T_i is experimentally estimated.

Co-funded by the European Union

SeaClear2.0 is co-funded by the European Union under the Horizon Europe Programme (Grant Agreement 101093822). Views and opinions expressed herein are those of the author(s) and do not necessarily reflect those of the European Union or European Climate, Infrastructure and Environment Executive Agency (CINEA). Neither the European Union nor the granting authority can be held responsible for them

Table 2: SeaCat2.0 USV dynamic model parameters.

Parameter	Variable	Value	Notes
Acceleration of gravity	g	9.81 m/s^2	
Water density	ρ	1025 kg/m^3	
Froude number	F_n	0.41	Displacement vessel [12]
Distance from O^b to CoG along x^b	x_g	0 m	
Maximum forward speed	u_max	3.09 m/s	6 knots
Total length of the boat	l_tot	5.7 m	
Total width of the boat	b_tot	2.0 m	
Draft	d	0.83 m	
Length of the two pontoons	l_pontoon	5.7 m	
Width of the two pontoons	b_pontoon	0.65 m	
Pontoon centerline distance from x^b	y_pontoon	0.79 m	
Displacement volume	∇	1.27 m^3	$\nabla = m/\rho$
Waterline area coefficient	c_w	0.89	Ratio between waterline area and pontoon area
Block coefficient	c_b	0.56	Ratio between pontoon volume and pontoon box
Mass	m	1300 kg	No LARS, full fuel tanks
Inertia w.r.t. z^b axis	I_z	2820 kg m^2	
Sway time constant	T_sway	10 s	Rough approximation, need real data for better estimate
Yaw time constant	T_yaw	10 s	Same as above
Bow thrusters angle from y^b axis	α	15°	
Bow thrusters distance from x axis	b_bow	0.8 m	
Stern thrusters distance from x axis	b_stern	0.8 m	
Bow thrusters distance from y axis	l_bow	2.1 m	
Stern thrusters distance from y axis	l_stern	2.4 m	
Added masses and hydrodynamic derivatives	$X_{\dot{u}}$	125 kg	$X_{\dot{u}} = 2.7\rho\nabla^{5/3}/l_\text{tot}^2$
	$Y_{\dot{v}}$	1950 kg	$Y_{\dot{v}} = 1.5m$
	$Y_{\dot{r}}$	0 kg	
	$N_{\dot{r}}$	4800 kg m^2	$N_{\dot{r}} = 1.7I_z$
	X_u	77 kg/s	$X_u = 24.4g/u_\text{max}$
	Y_v	325 kg/s	$Y_v = \boldsymbol{M}[2,2]/T_\text{sway}$
	Y_r	0 kg/s	
	N_v	0 kg/s	
	N_r	761 kg/s	$N_r = \boldsymbol{M}[3,3]/T_\text{yaw}$

Co-funded by the European Union

SeaClear2.0 is co-funded by the European Union under the Horizon Europe Programme (Grant Agreement 101093822). Views and opinions expressed herein are those of the author(s) and do not necessarily reflect those of the European Union or European Climate, Infrastructure and Environment Executive Agency (CINEA). Neither the European Union nor the granting authority can be held responsible for them

3.1.2 Dynamic positioning controllers

Following the approach used for the SeaCat USV in SeaClear, a PID controller is first developed. Given the dynamic model (16), where the motion of the SeaCat2.0 USV is decoupled in the three degrees of freedom surge, sway, and yaw, three PID controllers are designed, one for each DOF.

$$\boldsymbol{\tau}_i = k_{\mathrm{p},i} e_i + k_{\mathrm{d},i} \dot{e}_i + k_{\mathrm{i},i} \int_0^t e_i dt, \tag{19}$$

where $i \in \{\mathrm{surge}, \mathrm{sway}, \mathrm{yaw}\}$. Depending on the DOF being considered, the reference tracking errors are computed as $e_{\mathrm{surge}} = x_{\mathrm{ref}} - x$, $e_{\mathrm{sway}} = y_{\mathrm{ref}} - y$, and $e_{\mathrm{yaw}} = \psi_{\mathrm{ref}} - \psi$. The PID parameters in (19) can be tuned either manually or using the dynamic model (16). The resulting controller returns the force vector $\boldsymbol{\tau}_{\mathrm{control}}$, which is then converted to the thrusters input control vector $\boldsymbol{u}$ by solving problem (17), which results in the relation

$$\boldsymbol{u} = \boldsymbol{T}^{\dagger} \boldsymbol{\tau}_{\mathrm{control}},$$

where $\boldsymbol{T}^{\dagger} = \boldsymbol{W}^{-1}\boldsymbol{T}^{\top}(\boldsymbol{T}\boldsymbol{W}^{-1}\boldsymbol{T}^{\top})^{-1}$.

Motivated by the development of the dynamic model described in the previous section, a model-based controller is also developed. The controller is based on Model Predictive Control (MPC), where a discrete-time optimal control problem over an horizon of length N is solved at every time step. The first element of the solution is applied to the plant, and the optimal control problem is solved again at the next time step, in a receding-horizon fashion. The MPC controller has the advantage of being able to consider state and input constraints, such as a maximum power constraints for the thrusters, and can take into account the thrust allocation problem and the actuation delay, returning directly the thrusters control input $\boldsymbol{u}$. The MPC optimal control problem is formulated as

$$\begin{aligned} J(\boldsymbol{x}(t), \boldsymbol{x}_{\mathrm{ref}}(t)) = \min_{\bar{\boldsymbol{x}}(t), \bar{\boldsymbol{u}}(t)} & \sum_{k=1}^{N} ||\boldsymbol{x}_{\mathrm{ref}}(t) - \boldsymbol{x}(k|t)||_Q + ||\boldsymbol{u}(k|t)||_R, \\ \text{s.t. } & \boldsymbol{x}(0|t) = \boldsymbol{x}(t), \\ & \boldsymbol{x}(k+1|t) = f(\boldsymbol{x}(k|t), \boldsymbol{u}(k|t)), \\ & \boldsymbol{u}(k|t) \in \mathcal{U}, \end{aligned}$$

where N is the control horizon, $\bar{\boldsymbol{x}} = [\boldsymbol{x}^{\top}(1|t), \cdots, \boldsymbol{x}^{\top}(N+1|t)^{\top}]^{\top}$ is the predicted sequence of states of the system, and $\bar{\boldsymbol{u}} = [\boldsymbol{u}^{\top}(1|t), \cdots, \boldsymbol{u}^{\top}(N|t)^{\top}]^{\top}$ is the control sequence to apply over the horizon. Moreover, $f(\boldsymbol{x}, \boldsymbol{u})$ represents the discrete-time dynamics of the system (based on the dynamic model of (16), in case of a linear MPC, and of (15) in case of nonlinear MPC (NMPC)), Q and R are diagonal matrices to weight respectively the tracking error and the control effort, and $\mathcal{U}$ is the input set, which includes bounds on the input forces, a maximum power constraints on the thrusters forces (1-norm constraint), and rate constraints on the input forces to approximate the actuation delay (18).

Co-funded by the European Union

SeaClear2.0 is co-funded by the European Union under the Horizon Europe Programme (Grant Agreement 101093822). Views and opinions expressed herein are those of the author(s) and do not necessarily reflect those of the European Union or European Climate, Infrastructure and Environment Executive Agency (CINEA). Neither the European Union nor the granting authority can be held responsible for them

3.1.3 Simulations

Both a linear and nonlinear version of the MPC controller have been implemented for the dynamic positioning of the SeaCat2[4]. Two sets of experiments in a Python simulation environment are carried out to compare the two controllers. In the first, the station keeping of the SeaCat2 is evaluated, where a static and known water current is applied to the USV. The results of this experiment are shown in Figure 7. In the figure it can be observed how both the controllers align the heading of the USV with the current in order to lower the required control effort.

In the second experiment, the capabilities of the controller for setpoint regulation (reference point tracking) are evaluated. In this case, the target point to reach and maintain is placed at a point with an offset $(\Delta x, \Delta y) = (10\mathrm{m}, 6\mathrm{m})$ from the USV location. Additionally, a heading error of $\pi/4\mathrm{rad}$ is considered. A low intensity (known) water current is also considered. The results of this experiment are shown in Figure 8.

3.1.4 Conclusion

Two new controllers, a MPC and a NMPC have been implemented for the dynamic positioning and reference tracking control of the SeaCat2 USV. An initial set of experiments in a simulation environment has been carried out, showing promising results. In particular, the controllers are able to exploit the knowledge of the static water currents to predict the future behavior of the USV. However, since the MPC controllers are model-based, they require the model of the USV to be accurate enough. In this sense, the model used here, and in particular the parameters value, may require to be estimated more accurately, also requiring the tuning of the controller parameters.

The real-world evaluation and, if necessary, further improvement of the controllers, is part of the future work on the upgrade of the SeaCat2.0 USV control. Experimental data collected during the tests and trials being conducted will be used for the validation of the controllers in a simulation environment.

[4]The MPC optimal control problem has been modeled with cvxpy and solved with gurobi. The NMPC problem has been modeled with casadi and solved with ipopt.

Co-funded by the European Union

SeaClear2.0 is co-funded by the European Union under the Horizon Europe Programme (Grant Agreement 101093822). Views and opinions expressed herein are those of the author(s) and do not necessarily reflect those of the European Union or European Climate, Infrastructure and Environment Executive Agency (CINEA). Neither the European Union nor the granting authority can be held responsible for them

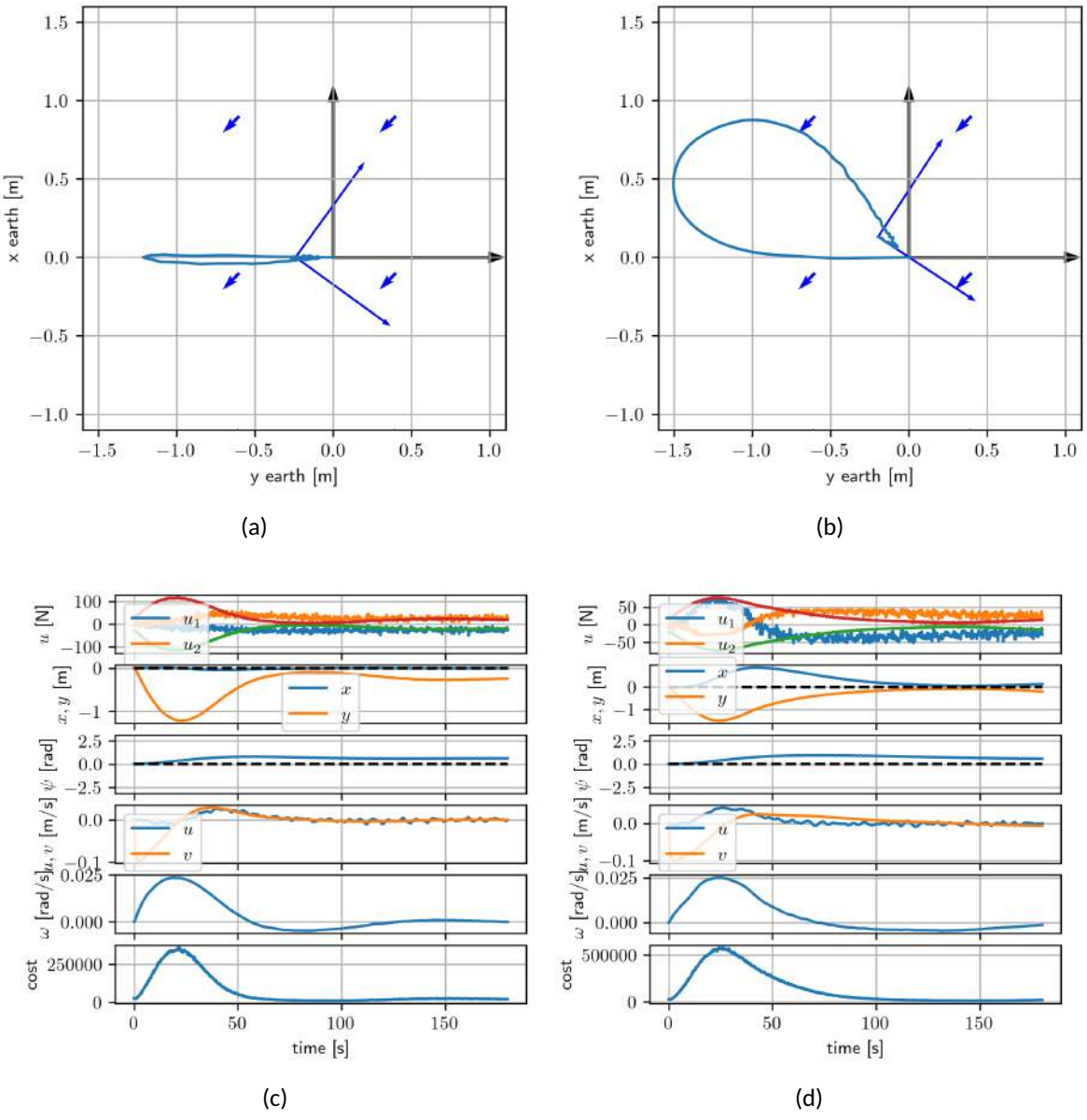


Figure 7: Results of the station keeping experiment. On the left-hand side, the results of the MPC controller. On the right-hand side, the results of the NMPC controller. In (a) and (b), the phase plot in the x-y reference plane. The black reference frame is the initial one, the blue one is the final one after 180s, and the light blue line is the trajectory followed by the USV. The blue arrows indicate the water current direction. In (c) and (d), the plots showing the state and input variables over time.

Co-funded by the European Union

SeaClear2.0 is co-funded by the European Union under the Horizon Europe Programme (Grant Agreement 101093822). Views and opinions expressed herein are those of the author(s) and do not necessarily reflect those of the European Union or European Climate, Infrastructure and Environment Executive Agency (CINEA). Neither the European Union nor the granting authority can be held responsible for them

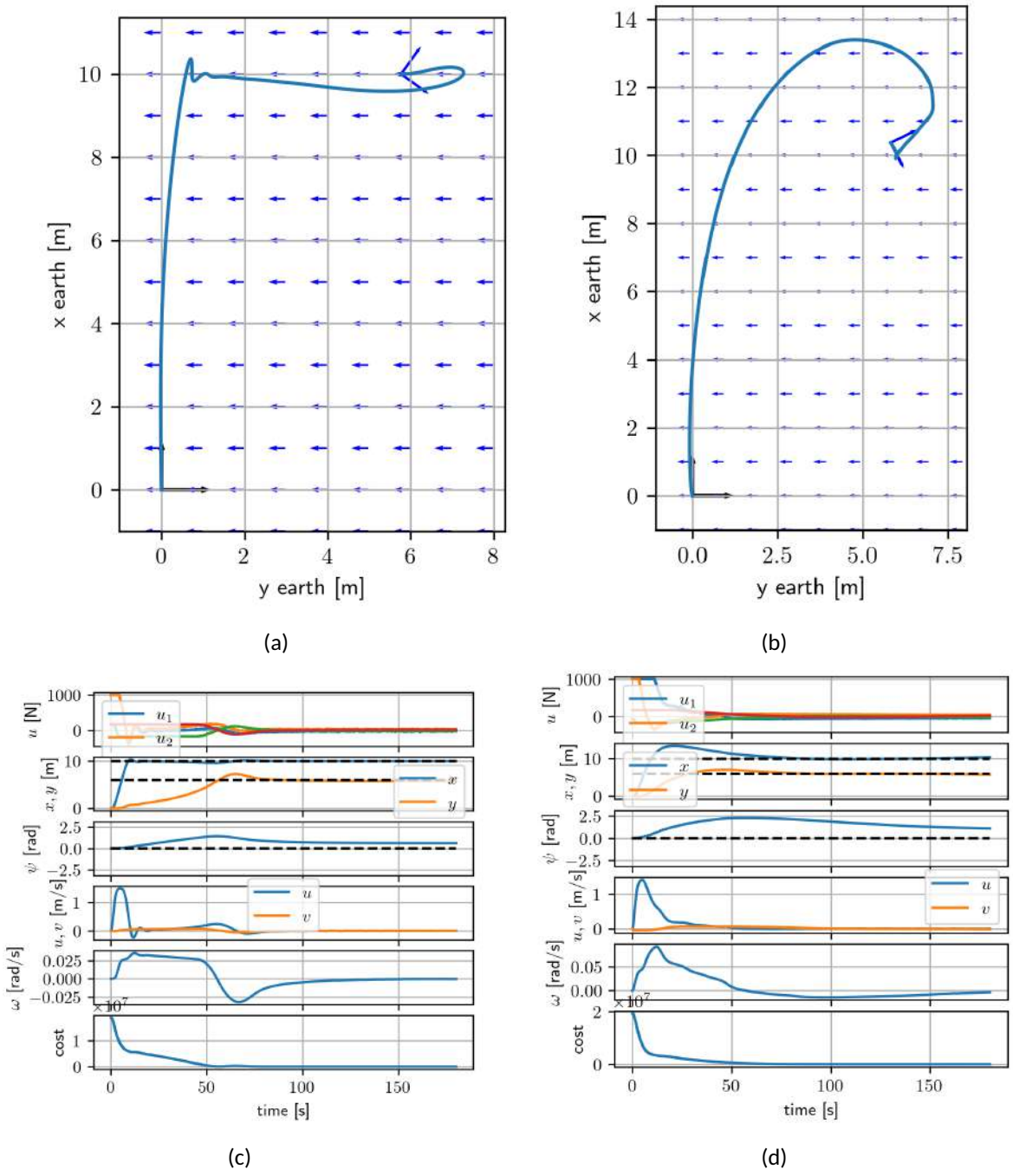


Figure 8: Results of the reference point tracking experiment. On the left-hand side, the results of the MPC controller. On the right-hand side, the results of the NMPC controller. In (a) and (b), the phase plot in the x-y reference plane. The black reference frame is the initial one, the blue one is the final one after 180s, and the light blue line is the trajectory followed by the USV. The blue arrows indicate the water current direction. In (c) and (d), the plots showing the state and input variables over time. Note that for the linear MPC, the water current speed had to be lowered (0.15m/s instead of 0.45m/s used in the NMPC case) as the controller would otherwise significantly overshoot the target point.

Co-funded by the European Union

SeaClear2.0 is co-funded by the European Union under the Horizon Europe Programme (Grant Agreement 101093822). Views and opinions expressed herein are those of the author(s) and do not necessarily reflect those of the European Union or European Climate, Infrastructure and Environment Executive Agency (CINEA). Neither the European Union nor the granting authority can be held responsible for them

3.2 SeaBees control

In this subsection we address the control of the SeaBees consisting of two small omnidirectional USV physically connected with a net whose aim is to collect floating litter within dynamic marine environment, see Fig 9. SeaBees are required to navigate obstacles, maintain a formation to optimize litter

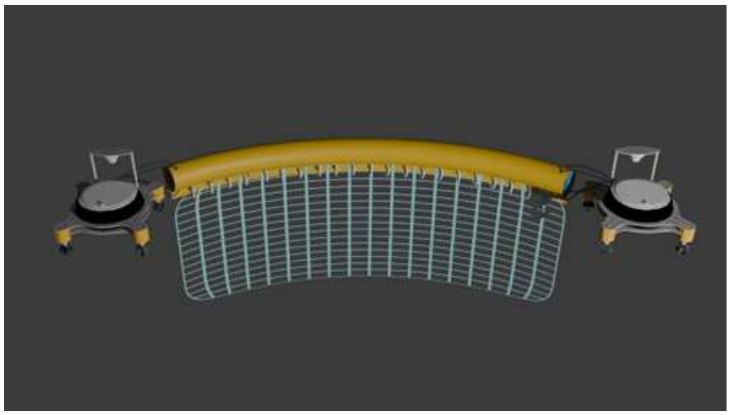


Figure 9: The SeaBees system: Two omnidirectional USVs physically connected with a collection net

collection efficiency, and manipulate the net to effectively capture floating debris. The dynamic nature of the marine environment, characterized by factors such as waves, winds, currents, and presence of other vessels, pose challenges for trajectory planning and control. Furthermore, variations in environmental conditions require adaptive control strategies to ensure robust performance. Initial level for the SeaBees control is WP tracking of the individual USV using a simple linear PID type of controller. During Hamburg trials, in May 2025, we used it to demonstrate a centralized line formation control for the SeaBees system with results shown on, Fig.10. In this section we describe the framework for decentralized optimal control based on MPC.



Figure 10: Centralized line formation control of SeaBees during the Hamburg pilot.

3.2.1 Modeling of Individual SeaBees

The dynamic equation incorporates a comprehensive model that combines both kinematic and dynamic elements, accounting for hydrodynamic forces and linear damping. This model is adapted to the low-speed nature of vehicles and the negligible pitch and roll movements. Moreover, the formulation inte-

Co-funded by the European Union

SeaClear2.0 is co-funded by the European Union under the Horizon Europe Programme (Grant Agreement 101093822). Views and opinions expressed herein are those of the author(s) and do not necessarily reflect those of the European Union or European Climate, Infrastructure and Environment Executive Agency (CINEA). Neither the European Union nor the granting authority can be held responsible for them

grates shared information among the USVs, contributing to collaborative and informed decision-making within the multi-agent system.

Each USV is modeled as a nonlinear dynamical system described by the following state-space equations:

$$\boldsymbol{\xi}_{k+1} = \mathbf{A}\boldsymbol{\xi}_k + \mathbf{B}u_k, \tag{20}$$

where $\boldsymbol{\xi}$ is the state vector representing the position, orientation, and velocity of the USV, $\mathbf{A}$ and $\mathbf{B}$ are state transition matrices, and u_k is the control input.

The state vector $\boldsymbol{\xi}$ is defined as:

$$\boldsymbol{\xi} = \begin{bmatrix} x \\ y \\ \psi \\ u \\ v \\ r \end{bmatrix}, \tag{21}$$

where x, y, and ψ represent the position and orientation in the global coordinate system, while u, v, and r denote the surge, sway, and yaw velocities, respectively.

The matrices $\mathbf{A}$ and $\mathbf{B}$ are linearized based on the kinematic and dynamic equations of the USV:

$$\mathbf{A}_i = \begin{bmatrix} 0 & 0 & -(\cos(\psi_{0,i}) \cdot u_{0,i} + \sin(\psi_{0,i}) \cdot v_{0,i}) & \cos(\psi_{0,i}) & \sin(\psi_{0,i}) & 0 \\ 0 & 0 & \cos(\psi_{0,i}) \cdot u_{0,i} - \sin(\psi_{0,i}) \cdot v_{0,i} & \sin(\psi_{0,i}) & \cos(\psi_{0,i}) & 0 \\ 0 & 0 & 0 & 0 & 0 & 1 \\ 0 & 0 & 0 & -\frac{D_v}{m} & 0 & 0 \\ 0 & 0 & 0 & 0 & -\frac{D_v}{m} & 0 \\ 0 & 0 & 0 & 0 & 0 & -\frac{D_r}{I} \end{bmatrix}, \tag{22}$$

where m is the mass of the USV, D_v is the hydrodynamic damping in surge and sway axes, D_r is the hydrodynamic damping in the yaw axis, and I is the moment of inertia of the USV.

The input matrix $\mathbf{B}$ is given by:

$$\mathbf{B}_i = \begin{bmatrix} 0 & 0 & 0 \\ 0 & 0 & 0 \\ 0 & 0 & 0 \\ \frac{1}{m} & 0 & 0 \\ 0 & \frac{1}{m} & 0 \\ 0 & 0 & \frac{1}{I} \end{bmatrix}, \tag{23}$$

The model also incorporates constraints to ensure safe and effective operation of the USVs. These constraints include:

Co-funded by the European Union

SeaClear2.0 is co-funded by the European Union under the Horizon Europe Programme (Grant Agreement 101093822). Views and opinions expressed herein are those of the author(s) and do not necessarily reflect those of the European Union or European Climate, Infrastructure and Environment Executive Agency (CINEA). Neither the European Union nor the granting authority can be held responsible for them

1. **Thrust Constraints**: The total thrust generated by the USVs must not exceed a certain limit to prevent excessive energy consumption and system wear.

$$\tau_u^2 + \tau_v^2 + \tau_r^2 \leq 1 \tag{24}$$

2. **Obstacle Avoidance Constraints**: The USVs are constrained to maintain a safe distance from obstacles to prevent collisions.

$$distance(\boldsymbol{X_i}, obs) \geq r_{obs} \tag{25}$$

3. **Model Constraints**: The dynamics and kinematics of the agents behave closely to the mathematical model.

$$\boldsymbol{\xi}_{k+l+1,i} = \mathbf{A}\boldsymbol{\xi}_{k+l,i} + \mathbf{B}u_{k+l,i}, \tag{26}$$

3.2.2 Model Predictive Control

The MPC framework is used to generate optimal control inputs for the USVs over a finite time horizon. The objective is to minimize a cost function that penalizes deviations from the desired trajectory, control effort, and violation of constraints. The cost function is defined as:

$$\begin{aligned} J_i = \sum_{l=0}^{N-1} \big[& \alpha_i \|\bar{\mathbf{x}}_{i,k+l} - \bar{\mathbf{x}}_{\text{ref},k+l}\|^2 + \gamma_i \|\mathbf{x}_{i,k+l} - \mathbf{x}_{j,k+l} - \mathbf{d}^*_{\text{ref}}\|^2 \\ & + \lambda_i (\|\mathbf{x}_{i,k+l} - \mathbf{x}_{j,k+l}\| - D_{ref})^2 + \mu_i (\psi_i - \psi_j)^2 \big] + \sum_{l=0}^{N-1} \left[\beta_i \|\mathbf{u}_{i,k+l}\|^2 + \sigma_i \|\Delta \mathbf{u}_{i,k+l}\|^2 \right], \end{aligned} \tag{27}$$

where $\bar{\mathbf{x}}$ represents the predicted state, $\bar{\mathbf{x}}_{\text{ref}}$ is the reference state, $\mathbf{x}$ is the actual state, $\mathbf{x}_j$ represents the state of neighboring USVs, $\mathbf{d}_{\text{ref}}$ is the desired inter-vehicle distance, $\mathbf{u}$ is the control input, and $\Delta\mathbf{u}$ is the change in control input.

The cost function consists of several terms:

1. $\alpha_i \|\bar{\mathbf{x}}_{i,k+l} - \bar{\mathbf{x}}_{\text{ref},k+l}\|^2$: Penalizes deviations of the predicted state from the reference state, ensuring that the USV follows the desired trajectory.

2. $\gamma_i \|\mathbf{x}_{i,k+l} - \mathbf{x}_{j,k+l} - \mathbf{d}^*_{\text{ref}}\|^2$: Penalizes deviations from the desired inter-vehicle distance between neighboring USVs, promoting formation stability.

3. $\lambda_i (\|\mathbf{x}_{i,k+l} - \mathbf{x}_{j,k+l}\| - D_{ref})^2$: Penalizes deviations from the desired inter-vehicle distance, ensuring that the USVs maintain a safe separation distance.

4. $\mu_i (\psi_1 - \psi_2)^2$: Penalizes deviations in the orientation of neighboring USVs, promoting alignment and coordination.

5. $\beta_i \|\mathbf{u}_{i,k+l}\|^2$: Penalizes control effort to ensure smooth and energy-efficient operation of the USVs.

6. $\sigma_i \|\Delta \mathbf{u}_{i,k+l}\|^2$: Penalizes abrupt changes in control inputs, ensuring smooth and stable control.

The MPC solves local problems while classical path planning algorithm like A* generates global path which is then given to MPC as references to follow. Global path planning only provides shortest path

Co-funded by the European Union

SeaClear2.0 is co-funded by the European Union under the Horizon Europe Programme (Grant Agreement 101093822). Views and opinions expressed herein are those of the author(s) and do not necessarily reflect those of the European Union or European Climate, Infrastructure and Environment Executive Agency (CINEA). Neither the European Union nor the granting authority can be held responsible for them

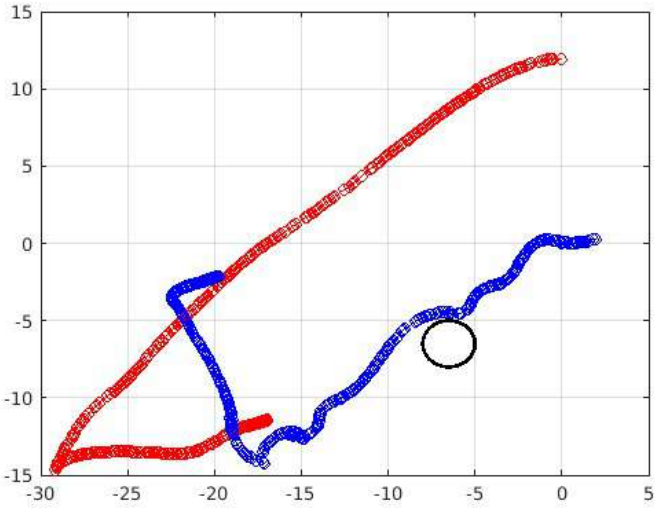


Figure 11: Simulation results in Matlab: The graph shows path of two USV (red and blue) in 2D (x-, y-) with both robots starting from an arbitrary initial position with the goal of reaching the final waypoints while maintaining a line formation and avoiding an obstacle (black).

traversable by at least one agent such as paths that are wide enough to allow passage of one or multiple agents in a file, while the MPC deals with possible needs for adjusting the formation to achieve such goals.

3.2.3 Simulation Results

Simulations were conducted to evaluate the performance of the proposed MPC approach in a simulated marine environment. The results demonstrate that the MPC controller effectively coordinates the movements of multiple USVs to achieve efficient litter collection while satisfying all constraints. Simulations were done in Matlab with promising results for obstacle avoidance, reference tracking and formation keeping.

The second part of the simulation was done using Matlab and ROS/Gazebo. Matlab is providing Gazebo with control inputs for robots and Gazebo is providing Matlab the position and velocity feedback. Matlab is running two MPCs and Gazebo is used as a physics simulator. The SeaBees system in Gazebo was modeled as two USVs physically connected with a net with mass and drag which was not part of the initial mathematical model. Simulations results with one obstacle are shown in Fig 11.

Another problem to consider are non-convex obstacles, as shown in Fig.12. With a small prediction horizon the MPC based controller cannot solve this and can get stuck in a local minima. To solve this we can increase the prediction horizon or we can find outer points and pull linear constraint such that the robot cannot enter the ”valley” which could be removed once the robot clears the obstacle.

Considering that we can only increase horizon so much before it starts to impact the performances we can also use global path planing to provide MPC with way points but unexpected nonconvex obstacles

Co-funded by the European Union

SeaClear2.0 is co-funded by the European Union under the Horizon Europe Programme (Grant Agreement 101093822). Views and opinions expressed herein are those of the author(s) and do not necessarily reflect those of the European Union or European Climate, Infrastructure and Environment Executive Agency (CINEA). Neither the European Union nor the granting authority can be held responsible for them

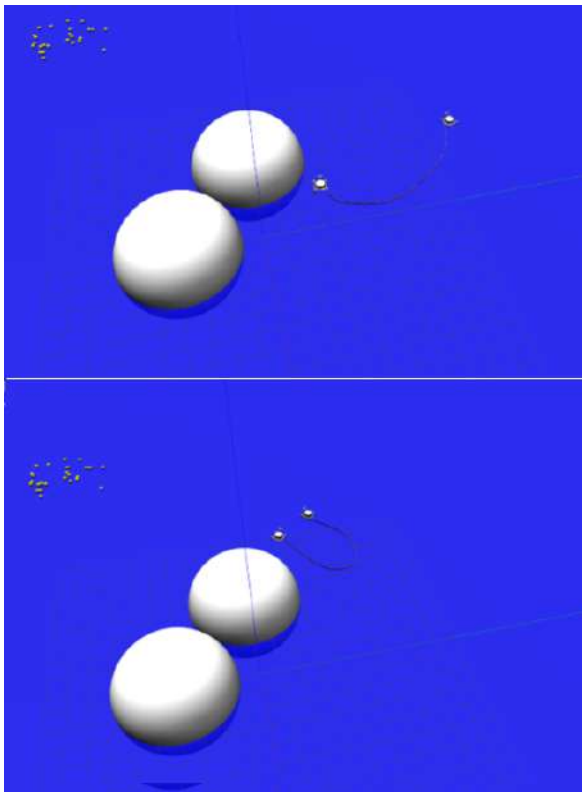


Figure 12: Validation of the developed algorithm in a more realistic simulation environment Gazebo. Using A* and MPC the SeaBees are able to overcome obstacles while maintaining the line formation.

could still cause problems.

3.2.4 Conclusion

This subsection presented a model predictive control approach for cooperative surface vehicles engaged in net-based litter collection. By integrating formation control, obstacle avoidance, and net manipulation constraints into the MPC framework, the proposed approach enables efficient and robust litter collection operations in dynamic marine environments.

Co-funded by the European Union

SeaClear2.0 is co-funded by the European Union under the Horizon Europe Programme (Grant Agreement 101093822). Views and opinions expressed herein are those of the author(s) and do not necessarily reflect those of the European Union or European Climate, Infrastructure and Environment Executive Agency (CINEA). Neither the European Union nor the granting authority can be held responsible for them

3.3 SeaDragon control

The SeaDragon USV is the shuttle tender uncrewed vessel, that sails from docks onto Seacat2 USV, for depositing the collected marine waste. Hence, it is a feature of the overall system for allowing interrupted collection. The system represents a significant improvement over the SeaClear system approach, which used a basket for litter collection. The basket approach presented several concerns including increased risk of entanglements, payload limitations due to vessel constraints and requisite torques for lifting from the seafloor, increased vulnerability to grounding incidents, prolonged operation duration requiring additional trips to shore, probability of requiring remapping efforts, and amplified total energy consumption.

3.3.1 USV hydrodynamic model

The shuttle tender USV is the in-house developed SeaDragon USV (see Figure 13), which is a $6.5\,\mathrm{m}$ x $2.2\,\mathrm{m}$ catamaran, having $350\,\mathrm{kg}$ payload and capable of developing up to $7\,\mathrm{kn}$ speed. The USV actuation system consists of a twin-azimuth propeller, capable of controlling the lateral drifts (on sway axis) and developing $6\,\mathrm{kW}$ power.

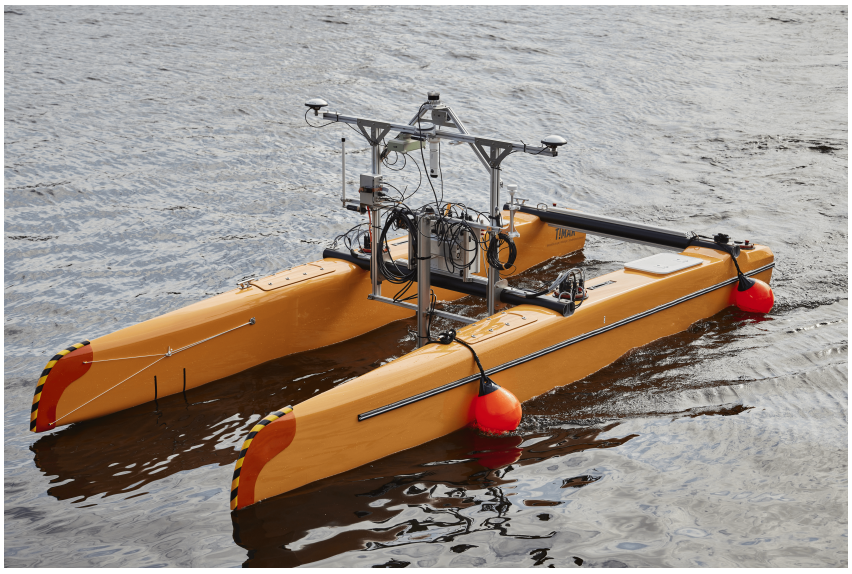


Figure 13: SeaDragon shuttle tender USV, catamaran used for validating the *Guidance* module

The complete Equations of Motion (EOM) for a 6 DOF system include multiple nonlinearities, such as hydrostatic effects, cross-flow drag, and nonlinear damping, but this representation is highly complex and suboptimal for controlling underactuated ships. Even with azimuth thrusters, there are only 4 control inputs (speed and angle of each thruster), while the heave motion (translation on the normal axis to the vessel) is not controllable. Therefore, a more appropriate linear 3 DOF horizontal plane model that only includes surge, sway, and yaw dynamics is used for the vessel model.

The *Froude Number* can be used to classify a surface vessel based on its maximal attainable velocity, as shown in Eq. 28, where U is the maximum surge velocity (in $\mathrm{m/sec}$) of the ship and L (in m) is its length.

Co-funded by the European Union

SeaClear2.0 is co-funded by the European Union under the Horizon Europe Programme (Grant Agreement 101093822). Views and opinions expressed herein are those of the author(s) and do not necessarily reflect those of the European Union or European Climate, Infrastructure and Environment Executive Agency (CINEA). Neither the European Union nor the granting authority can be held responsible for them

$$F_n = \frac{U}{\sqrt{gL}} \tag{28}$$

Based on [13] and assuming an $5.5\,\mathrm{m}$-long vessel with a top velocity of $4.63\,\mathrm{m/sec}$, this can be classified as a semi-displacement vessel with a Froude Number of 0.64, which means that neither buoyancy forces nor hydrodynamic forces are dominant with respect to providing the lift to maintain the ship afloat when moving at the maximum attainable surge velocity.

The forces and moments acting on a ship can be described using two distinct, established frameworks. The manoeuvring theory outlines the ship's motion at a steady speed U in calm waters, ignoring external disturbances, such as wave excitation. The hydrodynamic coefficients derived are constant and linear, allowing the entire system to be represented as a linear maneuvering model. The assumption of relatively calm waters aligns with port areas as the primary operating environment for the shuttle tender USV. On the other hand, station-keeping theory describes a ship's motion at zero or constant surge velocity and a fixed heading. This approach explicitly considers wave excitation and the resulting frequency-dependent potential coefficients.

The simplified 3 DOF USV model can be obtained under the following assumptions [14]:

- The vessel has three planes of symmetry.
- The mass distribution is homogeneous.
- The pitch and roll motions are neglected.

The three DOF kinematic equations can be described as follows:

$$\dot{\eta} = \begin{bmatrix} \cos\psi & -\sin\psi & 0 \\ \sin\psi & \cos\psi & 0 \\ 0 & 0 & 1 \end{bmatrix} \begin{bmatrix} u \\ v \\ r \end{bmatrix} = \mathbf{R}(\psi)\mathbf{v}. \tag{29}$$

Most ships have port/starboard symmetry but fore/aft non-symmetry. This non-symmetry leads to the nonzero off-diagonal terms in the inertia and damping matrices. However, these terms are small compared to the main diagonal terms [15].

Therefore, the dynamics equations of motion are given by [16]:

$$\mathbf{M}\dot{\mathbf{v}} = -\mathbf{C}(\mathbf{v})\mathbf{v} - \mathbf{D}\mathbf{v} + \tau + \mathbf{w}, \tag{30}$$

where the matrices $\mathbf{M}$, $\mathbf{C}(\mathbf{v})$ and $\mathbf{D}$ are given by:

$$\mathbf{M} = \begin{bmatrix} m_{11} & 0 & 0 \\ 0 & m_{22} & 0 \\ 0 & 0 & m_{33} \end{bmatrix}, \quad \mathbf{C}(\mathbf{v}) = \begin{bmatrix} 0 & 0 & -m_{22}v \\ 0 & 0 & m_{11}u \\ m_{22}v & -m_{11}u & 0 \end{bmatrix}, \quad \mathbf{D} = \begin{bmatrix} d_{11} & 0 & 0 \\ 0 & d_{22} & 0 \\ 0 & 0 & d_{33} \end{bmatrix}, \tag{31}$$

Co-funded by the European Union

SeaClear2.0 is co-funded by the European Union under the Horizon Europe Programme (Grant Agreement 101093822). Views and opinions expressed herein are those of the author(s) and do not necessarily reflect those of the European Union or European Climate, Infrastructure and Environment Executive Agency (CINEA). Neither the European Union nor the granting authority can be held responsible for them

where

$$m_{11} = m - X_{\dot{\mathbf{u}}}, \quad m_{22} = m - Y_{\dot{\mathbf{v}}}, \quad m_{33} = I_{\mathbf{z}} - N_{\dot{\mathbf{r}}}, \tag{32}$$

$$d_{11} = -X_{\mathbf{u}}, \quad d_{22} = -Y_{\mathbf{v}}, \quad d_{33} = -N_{\mathbf{r}}. \tag{33}$$

With the physical vessel being a prototype, only some of the parameters of the SeaDragon USV, the shuttle tender USV, could be estimated. These are summarised in Table 3.

Table 3: SeaDragon, the shuttle tender USV, estimated model parameters

SeaDragon USV Parameters	
Parameter Description	**Value**
Length (L)	$5.5\,\mathrm{m}$
Length of Waterline (L_{wl})	$5.5\,\mathrm{m}$
Weight of the Vessel	$360\,\mathrm{kg}$
Beam (B)	$2.2\,\mathrm{m}$
Payload mass (m_p)	$350\,\mathrm{kg}$
Payload location w.r.t. to COG	[-1.5 0 0] m
Centre of Gravity w/o equipment(rg)	[2, 0, 0.0] m
Yaw Time Constant (T_{yaw})	$3.236\,\mathrm{s}$
Maximum Forward Speed (U_{max})	$7\,\mathrm{knot}$
Maximum Static Forward Thrust (T_{max})	$31\,\mathrm{kg}$
Maximum Static Backwards Thrust (T_{min})	$-31\,\mathrm{kg}$
Centerline to Waterline Centroid (y_{pont})	$0.9\,\mathrm{m}$
Waterline Area Coefficient Cw_{pont}	0.7883
Block Coefficient Cb_{pont}	0.8998
Draft (front) d_f	$0.10\,\mathrm{m}$
Draft (back) d_b	$0.21\,\mathrm{m}$

The vessel design report completed in [17] contains the extended information on the vessel's modeling, including the complete sensor selection and technical specifications.

Co-funded by the European Union

SeaClear2.0 is co-funded by the European Union under the Horizon Europe Programme (Grant Agreement 101093822). Views and opinions expressed herein are those of the author(s) and do not necessarily reflect those of the European Union or European Climate, Infrastructure and Environment Executive Agency (CINEA). Neither the European Union nor the granting authority can be held responsible for them

3.3.2 Autonomous docking procedure

This section describes the workflow for achieving autonomous docking from a user-defined position onto the stern of SeaCat2 USV. The complete details of the software architecture, design and implementation can be found in [18].

Initially, the shuttle tender USV will be kept in an `idle` state until the marine litter phase is being commenced. Then, knowing the position of the SeaCat USV and having a priori information about the surrounding area via nautical chart data, a path will be planned. Depending on the vessel traffic, anchored ships, or other infrastructural elements not available in the nautical chart data, the path will be adapted "on the fly" during navigation. During navigation, the shuttle tender USV will be in the `path following` mode, or state, where the control objective of the autopilot is to steer the USV to converge to the series of waypoints with the final one, being placed next to the SeaCat USV's position. If the latter drifts from the initially recorded position, then the path will be adapted "on the fly", similar to when an unmapped obstacle is encountered.

Upon reaching the destination, the state will change to the `docking` mode, in which the reference points of the stern of the SeaCat 2 USV will be used to define a target pose relative to it, which can be regarded as safe for proceeding to the litter transboarding phase. In that sense existing guides, such as ones depicted in Figure 14, can be used for positioning the shuttle tender USV relative to the SeaCat 2 USV.

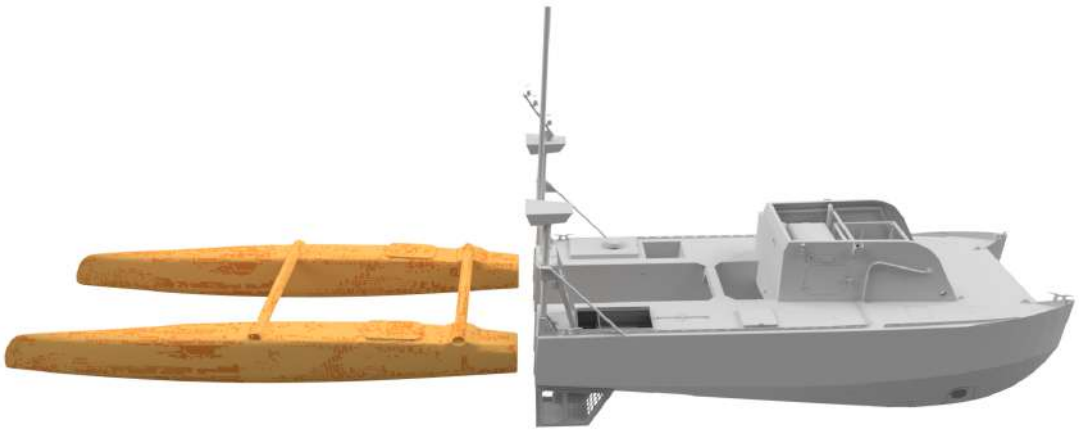


Figure 14: The stern of the SeaCat 2 USV has some reference guides for the stern-to-stern docking of the shuttle tender USV, which allow around $20\,\mathrm{cm}$ lateral tolerance (source SST)

Shortly after entering the litter transboarding phase, the shuttle tender USV will enter a `station keeping` state, which minimises all drifts from the pose (position and orientation) and gently pushes against the stern of the SeaCat 2 USV.

After completing the litter transboarding from the SeaCat USV to the shuttle tender USV, another path will be generated to reach the shore and discharge the litter. The complete set of states and transitions within the shuttle tender USV's mode of operation are depicted in Figure 15.

Co-funded by the European Union

SeaClear2.0 is co-funded by the European Union under the Horizon Europe Programme (Grant Agreement 101093822). Views and opinions expressed herein are those of the author(s) and do not necessarily reflect those of the European Union or European Climate, Infrastructure and Environment Executive Agency (CINEA). Neither the European Union nor the granting authority can be held responsible for them

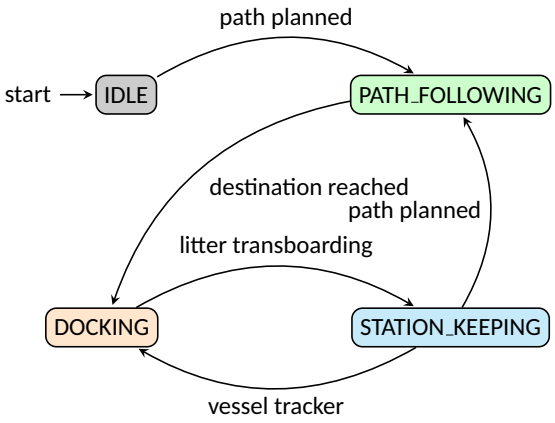


Figure 15: Operational states of the shuttle tender USV

For completeness, after discharging the litter at shore, the shuttle tender USV will plan a path to return to a predefined waiting area, where it will enter the `idle` state again, until being called for another marine litter collection mission.

3.3.3 Simulation results

The simulation environment for the shuttle tender USV is built using Gazebo, a popular open-source robotics simulator. The simulation environment includes a detailed model of the shuttle tender USV, as well as a realistic representation of the marine environment, including water currents, waves, and obstacles. The simulation environment also includes a virtual representation of the SeaCat 2 USV, which is used for testing the docking and litter transboarding procedures. The simulation environment is designed to be flexible and extensible, allowing for the testing of different scenarios and configurations.

Several scenarios have been developed within the simulation environment to test the various functionalities of the shuttle tender USV. These scenarios can be selected and extended in the interface which prompts the user when starting the simulation. The interface is depicted in Figure 16.

With the mathematical model of the shuttle tender USV being similar to the actual vessel, the simulation environment can replicate the dynamics and behaviour of the vessel in different conditions. The weights of the controllers and the parameters for transitioning to other states could be tuned first time without the need of a physical sea trial, thus reducing the time and risks associated with field testing. Nevertheless, the fine tuning of the weights and parameters, and the software pipeline validation still required sea trials. And even if the visual representation of the vessel is not photorealistic, as it can be seen in Figure 17, these still give enough insight about the operation and for the possible limitations of the system.

The whole operation can be monitored via Foxglove Studio, using the appropriate widget layout, as seen in Figure 18.

Co-funded by the European Union

SeaClear2.0 is co-funded by the European Union under the Horizon Europe Programme (Grant Agreement 101093822). Views and opinions expressed herein are those of the author(s) and do not necessarily reflect those of the European Union or European Climate, Infrastructure and Environment Executive Agency (CINEA). Neither the European Union nor the granting authority can be held responsible for them

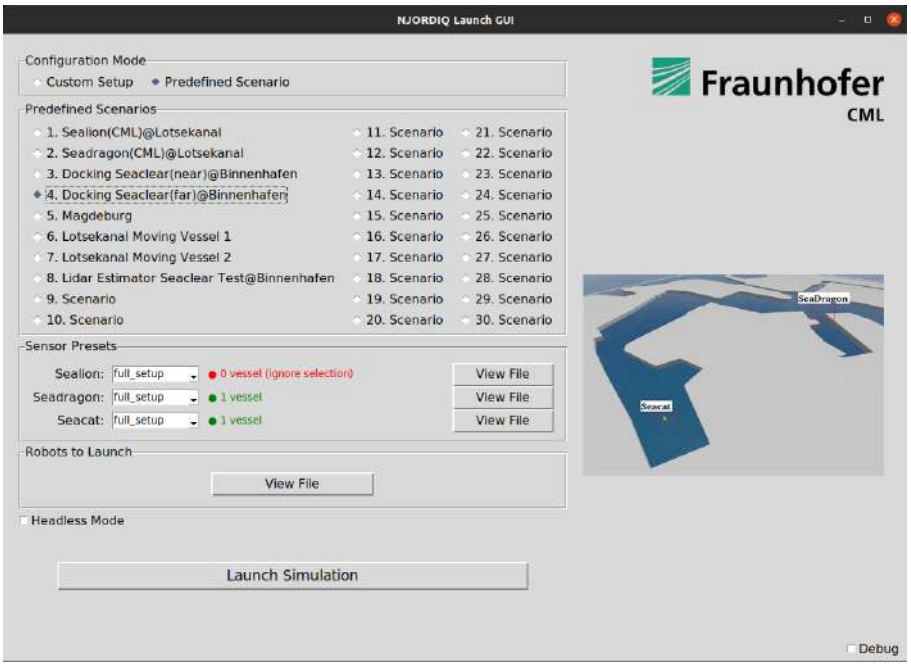


Figure 16: Simulation interface for selecting and extending scenarios for testing the shuttle tender USV

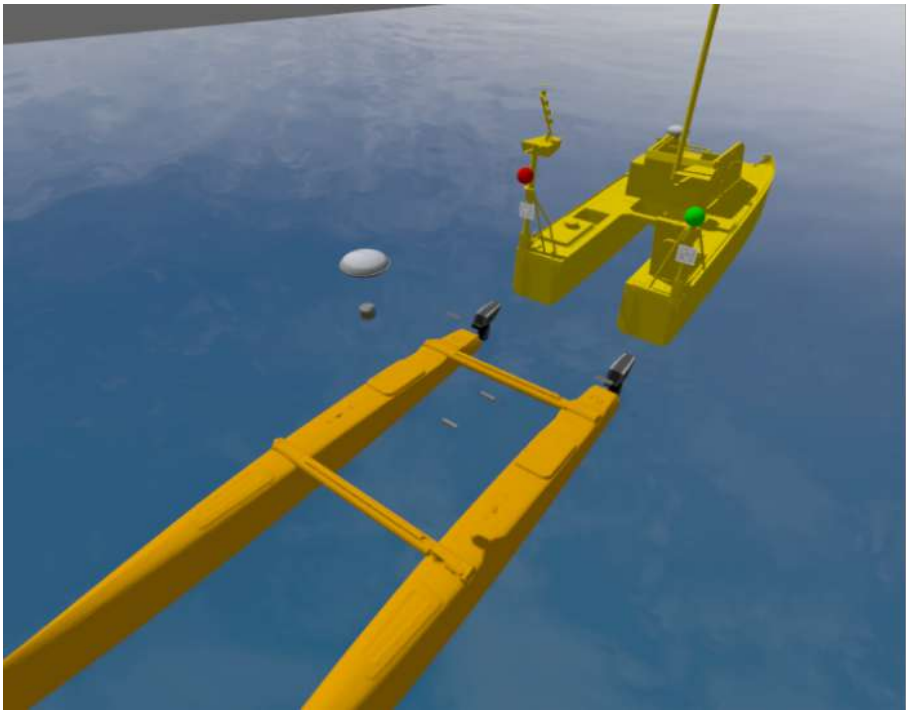


Figure 17: Docking procedure simulation between the shuttle tender USV and the SeaCat 2 USV within the Gazebo environment

Co-funded by the European Union

SeaClear2.0 is co-funded by the European Union under the Horizon Europe Programme (Grant Agreement 101093822). Views and opinions expressed herein are those of the author(s) and do not necessarily reflect those of the European Union or European Climate, Infrastructure and Environment Executive Agency (CINEA). Neither the European Union nor the granting authority can be held responsible for them

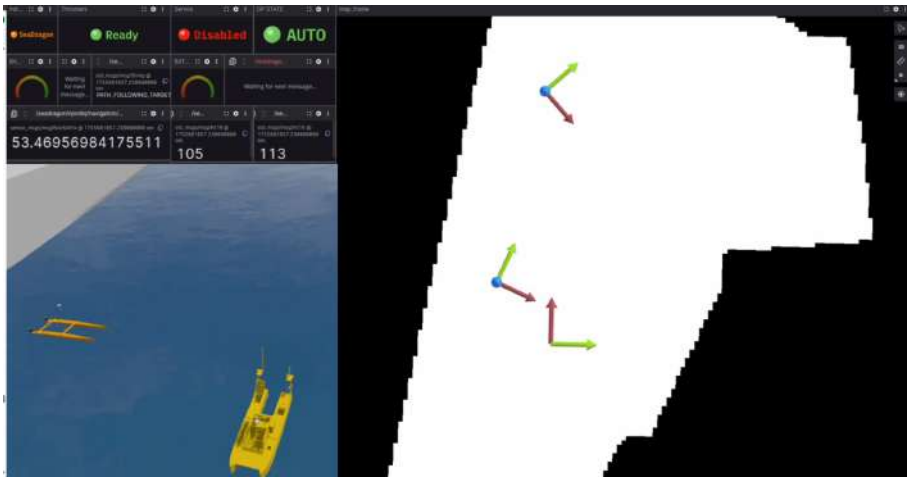


Figure 18: SeaDragon USV's command and control dashboard (in Foxglove Studio, coupled with the SeaClear2.0 digital twin, source Fraunhofer CML)

3.3.4 Experimental results

Following the simulation results, the logic has been tested through several sea trials and, ultimately, via the full system demonstrations within three locations. The performance and the key outcomes of the experiments have been discussed in [18].

Because the presence of the SeaCat 2 USV is essential for the testing but couldn't be guaranteed at all times, a mock target USV was also designed and built to simulate the presence of the SeaCat 2 USV during the tests. The mock target USV is equipped with a Global Navigation Satellite System (GNSS) system to provide positioning information, which is then transmitted to the shuttle tender USV in the same way as the SeaCat 2 USV. The mock target USV also has a physical structure that mimics the stern of the SeaCat 2 USV, allowing for realistic docking tests.

The experiments have been conducted in the Pilot's channel area, as depicted in Figure 19. The channel is situated in the southern part of the port city behind a lock that protects it from most of the currents of the Elbe River. Consequently, many of the tidal effects and currents were mitigated. On average, the currents in the Elbe are approximately $1.2\,\mathrm{m/sec}$ or $2.3\,\mathrm{kn}$. Most disturbances are caused by the wind, which during sea trials has been blowing at a speed of $6\,\mathrm{m/sec}$ to $8\,\mathrm{m/sec}$, or $11\,\mathrm{kn}$ to $16\,\mathrm{kn}$. The wind direction was N, NE, and E, depending on the day.

Due to its lack of actuation and impossibility to anchor in the test sites, the mock target USV is towed by a crewed vessel during the tests, in this case a Rigid Inflatable Boat (RIB), ensuring it remains stationary during the docking procedure. The RIB tightly binds the mock target USV to one of its inflatables, while it being positioned next to the quay wall, in order mimic the same damping characteristics as the SeaCat 2 USV. The experiments with the mock target USV are depicted in Figure 20. The main difference to the SeaCat 2 USV is the absence of the inflatables, which, on one hand, limits the possibility of side drifting when the vessels are docked, but, on the other hand, allow the sway error to be compensated even in the last centimeters before reaching the final docking position. As the inflatables on the Seacat 2 USV extend around $25\,\mathrm{cm}$ outwards, the sway error needs to be within the tolerance before encountering them.

Co-funded by the European Union

SeaClear2.0 is co-funded by the European Union under the Horizon Europe Programme (Grant Agreement 101093822). Views and opinions expressed herein are those of the author(s) and do not necessarily reflect those of the European Union or European Climate, Infrastructure and Environment Executive Agency (CINEA). Neither the European Union nor the granting authority can be held responsible for them

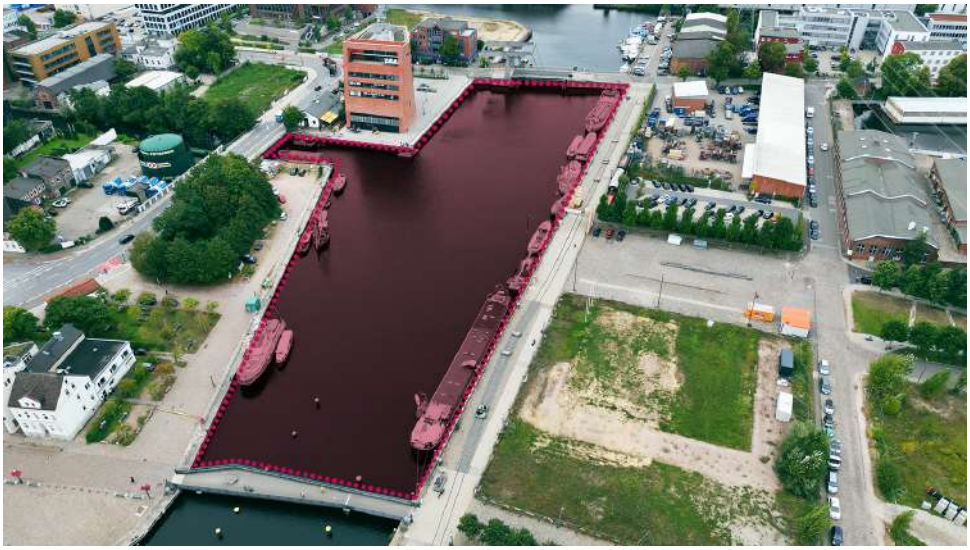


Figure 19: Lotsekanal (Pilot's Channel) in the Port of Hamburg, selected sea trials area and possible SeaClear2.0 pilot site.



Figure 20: Experiments with the mock target USV being towed by a crewed vessel in the Pilot's Channel. The shuttle tender USV approaches the mock target USV for docking tests

Co-funded by the European Union

SeaClear2.0 is co-funded by the European Union under the Horizon Europe Programme (Grant Agreement 101093822). Views and opinions expressed herein are those of the author(s) and do not necessarily reflect those of the European Union or European Climate, Infrastructure and Environment Executive Agency (CINEA). Neither the European Union nor the granting authority can be held responsible for them

The SeaDragon USV has been successfully tested by the date of writing in 3 locations: Hamburg, Marseille and Dubrovnik. In each of the aforementioned locations, the vessels maintains a safe distance of $40\,\mathrm{m}$ to $60\,\mathrm{m}$ from the SeaCat2 when not actively docking.



Figure 21: Docking procedure for litter transboarding between the SeaCat 2 USV and the shuttle tender USV. The shuttle tender USV approaches the stern of the SeaCat 2 USV and aligns within the two inflatables onboard the latter.

When the litter bay reaches its payload capacity, the SeaDragon sails back to shore for discharging. As depicted in Figure 22a and in Figure 22b, the vehicle completed its task regardless of the type of litter and the location in which it was deployed.

3.3.5 Conclusions

The SeaDragon shuttle tender USV was presented as a key enabler for uninterrupted marine litter collection, superseding the basket-based SeaClear approach and mitigating its associated risks (entanglement, payload and torque limits, grounding, and energy overhead). A linear 3 DOF surge–sway–yaw maneuvering model was adopted, justified by the vessel's actuation and its semi-displacement regime ($F_n = 0.64$). Given prototype constraints, a best-practice identification yielded the parameter set in Table 3, trading completeness for feasibility.

The autonomous docking workflow was formalised as a finite-state machine (`idle`, `path_following`, `docking`, `station_keeping`), enabling stern-to-stern approach within the $20\,\mathrm{cm}$ lateral tolerance imposed by the SeaCat 2 inflatables. Gazebo-based simulation permitted first-pass tuning of controller weights and state-transition parameters without sea trials, though field validation remained necessary for fine-tuning and pipeline verification.

Co-funded by the European Union

SeaClear2.0 is co-funded by the European Union under the Horizon Europe Programme (Grant Agreement 101093822). Views and opinions expressed herein are those of the author(s) and do not necessarily reflect those of the European Union or European Climate, Infrastructure and Environment Executive Agency (CINEA). Neither the European Union nor the granting authority can be held responsible for them



(a) Collected litter in the Port of Marseille (b) Collected litter next to Uvala Beach in Dubrovnik

Figure 22: SeaDragon USV collection of marine litter validation in public demonstrations

Sea trials in Hamburg, Marseille, and Dubrovnik confirmed robust performance under realistic disturbances (winds of $6\,\mathrm{m\,s^{-1}}$ to $8\,\mathrm{m\,s^{-1}}$), with successful docking against a towed mock target and reliable litter transboarding and discharge across litter types and sites. These results validate the docking logic and demonstrate the operational readiness of the shuttle tender concept, while identifying sway-error compensation within the inflatable clearance as the principal precision constraint for future refinement.

Co-funded by the European Union

SeaClear2.0 is co-funded by the European Union under the Horizon Europe Programme (Grant Agreement 101093822). Views and opinions expressed herein are those of the author(s) and do not necessarily reflect those of the European Union or European Climate, Infrastructure and Environment Executive Agency (CINEA). Neither the European Union nor the granting authority can be held responsible for them

4 ROV control upgrade

4.1 Observation ROV

During the SeaClear project we developed a decoupled, cascaded PID control strategy for the observation ROV. Figures 23 and 24 present illustrative results obtained by porting this decoupled control logic from ROS to ROS2 and applying it to track the lawnmower-shaped trajectories required for the mapping process. The ROV manages to accurately reach the desired waypoints in 2D. However, Figure 24 shows that the orientation and depth of the ROV are not very accurately controlled during the execution of the lawnmower trajectory. More importantly, the lawnmower trajectory was executed using a constant depth reference and with a fixed yaw independent of the lawnmower orientation. Therefore, in this section, we describe two ideas to upgrade the control used for the observation ROV. The first is to replace the decoupled, cascaded PID-controllers with an optimal control strategy, for which we describe the approach used to approximate the model of the observation ROV in Section 4.1.1; and describe the optimal control framework used to design the controller, with results, in Section 4.1.2. The second idea (Sections 4.1.4-4.1.5) is to improve the PID control strategy for better sensing, by (a) maintaining a constant altitude above the seafloor, rather than a constant depth; and (b) having the yaw change with the lawnmower's orientation.

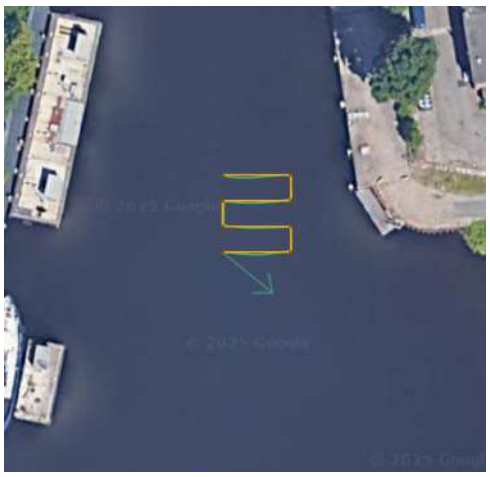


Figure 23: Lawnmower trajectory performed by the observation ROV during the Hamburg pilot.

4.1.1 Modelling of the observation ROV

Most optimal control approaches require a known model of the controlled system. Therefore, we must find an approximate model of the observation ROV. We chose the model proposed in [9] for underwater vehicles:

$$M\dot{\nu} + C(\nu)\nu + D(\nu)\nu + g(\eta) = \tau \tag{34}$$

$$\dot{\eta} = J(\eta)\nu \tag{35}$$

Co-funded by the European Union

SeaClear2.0 is co-funded by the European Union under the Horizon Europe Programme (Grant Agreement 101093822). Views and opinions expressed herein are those of the author(s) and do not necessarily reflect those of the European Union or European Climate, Infrastructure and Environment Executive Agency (CINEA). Neither the European Union nor the granting authority can be held responsible for them

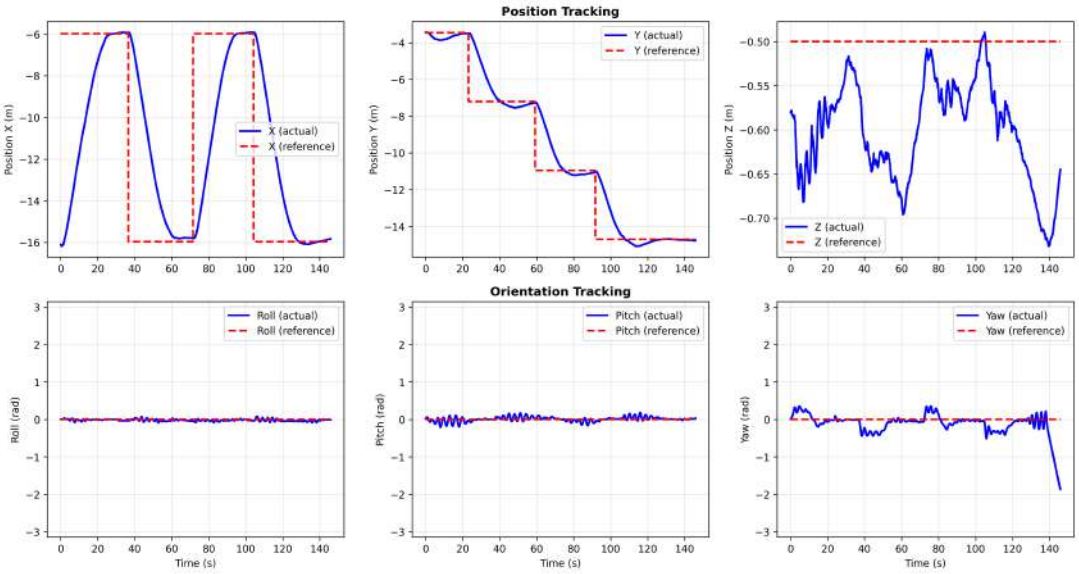


Figure 24: Trajectory tracking performance of the observation ROV using the original PID control strategy. Corresponds to the 2D plot in Figure 23.

where:

- $\eta = [x, y, z, \phi, \theta, \psi]^\top$ includes the position in the inertial frame $p = [x, y, z]^\top$ and the Euler angles: $\Theta = [\phi, \theta, \psi]^\top$.
- $\nu = [u, v, w, p, q, r]^\top$ includes the body-fixed linear and angular velocities.
- M is the inertia matrix, which combines the rigid-body and the added mass terms, i.e. $M = M_{RB} + M_A$.
- $C(\nu)$ is the Coriolis-centripetal matrix, which is also the sum of a rigid-body and an added-mass component $C(\nu) = C_{RB}(\nu) + C_A(\nu)$.
- $D(\nu)$ are the damping parameters.
- $g(\eta)$ are the restoring forces.

The parameters required to approximate the restoring forces $g(\eta)$ and the rigid-body forces $M_{RB}\dot{\nu}$ and $C_{RB}(\nu)\nu$ were determined based on the CAD model of the observation ROV. For the hydrodynamic forces $M_A\dot{\nu}$, $C_A(\nu)\nu$, and $D(\nu)\nu$ we follow the example presented in [19] and approximate them using a decoupled model, i.e. $D(\nu)$ and M_A are diagonal matrices. To this end, we collected experimental datasets and identified the parameters using linear regression, following the protocol proposed in [19]:

- for the damping parameters we collected data by iteratively sending constant wrench commands to the observation ROV for each DOF. The nonlinear damping coefficients are approximated using a linear and a quadratic component, i.e. $D(\nu)\nu \approx D_L\nu + D_Q(\nu \odot |\nu|)$, where $\odot$ is the element-wise product.

Co-funded by the European Union

SeaClear2.0 is co-funded by the European Union under the Horizon Europe Programme (Grant Agreement 101093822). Views and opinions expressed herein are those of the author(s) and do not necessarily reflect those of the European Union or European Climate, Infrastructure and Environment Executive Agency (CINEA). Neither the European Union nor the granting authority can be held responsible for them

- for the added mass parameters we collected data by iteratively sending sinuisoidal wrench commands to the observation ROV. Note that since we do not have any sensors measuring angular accelerations, the identified M_A has non-zero values only for the linear accelerations. Nonetheless, due to the fact the rigid-body term M_{RB} is a full matrix, the inertia matrix M remains invertible which is required for the dynamic system to remain meaningful.

4.1.2 LQT control for the observation ROV

Linear Quadratic Tracking (LQT) [20] controllers are a type of optimal controllers that given a linear dynamic system:

$$\dot{x} = Ax + Bu \tag{36}$$
$$y = Cx \tag{37}$$

aim to optimize the control sequence $U^* = \{u^*(t)|t \in [0, T]\}$ in order to minimize the finite-horizon cost function:

$$J = \frac{1}{2}\int_0^T \left[(y(t) - r(t))^\top Q(y(t) - r(t)) + u(t)^\top Ru(t)\right] dt + \frac{1}{2}(y(T) - r(T))^\top Q_T(y(T) - r(T)) \tag{38}$$

and thereby ensure that the outputs $y(t)$ track the references $r(t)$.

The main objective of the observation ROV is waypoint following for exploration of the environment. This involves following a reference trajectory for the positions while also maintaining a stable orientation in order to generate a meaningful sequence of observations. To achieve this, considering the state variables $x = [\eta^\top, \nu^\top]^\top$, the input $u = \tau$, and a linearization of the model described above, we can design an LQT controller for the observation ROV. In order to linearize the model of the ROV we first rearrange it as:

$$\begin{bmatrix}\dot{\eta}\\ \dot{\nu}\end{bmatrix} = \begin{bmatrix}f_1(\eta,\nu)\\ f_2(\eta,\nu)\end{bmatrix} + \begin{bmatrix}0\\ f_3(u)\end{bmatrix} = \begin{bmatrix}J(\eta)\nu\\ -M^{-1}[C(\nu)\nu + D_L\nu + D_Q\mathrm{diag}(|\nu|)\odot\nu + g(\eta)]\end{bmatrix} + \begin{bmatrix}0\\ M^{-1}u\end{bmatrix} \tag{39}$$

Using this formulation we can approximate the dynamics of the model using Taylor series expansion around the operating point $\dot{x}_0 = f(\eta_0, \nu_0, u_0)$ as:

$$\begin{bmatrix}\dot{\eta} - \dot{\eta_0}\\ \dot{\nu} - \dot{\nu_0}\end{bmatrix} = \begin{bmatrix}\frac{\partial f_1}{\partial \eta}\Big|_{\eta=\eta_0,\nu=\nu_0} & \frac{\partial f_1}{\partial \nu}\Big|_{\eta=\eta_0,\nu=\nu_0}\\ \frac{\partial f_2}{\partial \eta}\Big|_{\eta=\eta_0,\nu=\nu_0} & \frac{\partial f_2}{\partial \nu}\Big|_{\eta=\eta_0,\nu=\nu_0}\end{bmatrix}\begin{bmatrix}\eta - \eta_0\\ \nu - \nu_0\end{bmatrix} + \begin{bmatrix}0\\ \frac{\partial f_3}{\partial u}\Big|_{u=u_0}\end{bmatrix}(u - u_0) \tag{40}$$

Due to the fact that for the mapping processes the desired orientation is generally $\Theta = [0, 0, 0]^\top$ and the nonlinearities of the model do not depend on the position of the ROV we chose $p_0 = [0, 0, 0]^\top$. Furthermore $f_3(u)$ from (39) is already linear in u. The litter detection from imaging sensors requires a relatively slow motion of the ROV. Therefore, for the linearization we choose the velocity vector $\nu_0 =$

Co-funded by the European Union

SeaClear2.0 is co-funded by the European Union under the Horizon Europe Programme (Grant Agreement 101093822). Views and opinions expressed herein are those of the author(s) and do not necessarily reflect those of the European Union or European Climate, Infrastructure and Environment Executive Agency (CINEA). Neither the European Union nor the granting authority can be held responsible for them

$[0, 0, 0, 0, 0, 0]^\top$. As a result, by considering the terms that simplify due to the zero operating point, we get the matrices that define the linear state-space model for the ROV:

$$A = \begin{bmatrix} 0 & J(\eta_0) \\ -M^{-1} \left.\frac{\partial g}{\partial \eta}\right|_{\eta=\eta_0} & -M^{-1} D_L \end{bmatrix} \tag{41}$$

$$B = \begin{bmatrix} 0 \\ M^{-1} \end{bmatrix} \tag{42}$$

$$C = \begin{bmatrix} I_6 & 0_{6\times 6} \end{bmatrix} \tag{43}$$

where the structure of the output matrix C reflects the fact that the control objectives are waypoint-tracking and the stabilization of the orientation.

The solution of the LQT problem can be derived using a dynamic programming approach, by introducing a quadratic cost-to-go function:

$$V(x,t) = \frac{1}{2} x^\top P(t) x - x^\top g(t) + h(t) \tag{44}$$

and using the Hamilton-Jacobi-Bellman equation:

$$-\frac{\partial V(x,t)}{\partial t} = \min_u \left[\frac{1}{2}(y-r)^\top Q (y-r) + \frac{1}{2} u^\top R u + \frac{\partial V}{\partial x} \dot{x} \right] \tag{45}$$

For the finite-horizon LQT problem, the gain matrices used to compute $u^*(t)$ are time-varying and depend on the values of $P(t)$ and $g(t)$:

$$u^*(t) = -Kx(t) - K_r \tag{46}$$

$$K = R^{-1} B^\top P(t) \tag{47}$$

$$K_r = R^{-1} B^\top g(t) \tag{48}$$

Note that the control input $u^*(t)$ has a state-feedback component $u_x = -Kx(t)$ for the stabilization problem and a feedforward component $u_r = -K_r$ that accounts for the non-zero reference r.

Computing the sequence of optimal inputs U^* involves integrating the solutions of a series of algebraic Riccati equations backwards in time in order to iteratively compute the coefficients of the cost-to-go function $V(x,t)$:

$$-\dot{P} = A^\top P + PA - PBR^{-1}B^\top P + C^\top Q C \tag{49}$$

$$-\dot{g} = (A - BR^{-1}B^\top P)^\top g + C^\top Q r \tag{50}$$

$$-\dot{h} = -\frac{1}{2} g^\top B R^{-1} B^\top g + \frac{1}{2} r^\top Q r \tag{51}$$

As a computationally cheaper alternative, we can approximate the solution using the infinite horizon version of the LQT problem. Therefore, when $T \to \infty$, we can approximate the coefficients of the cost-to-go function with constant values, i.e. $P(t) \approx P_\infty$ and $g(t) \approx g_\infty$. As a result, the controller can be

Co-funded by the European Union

SeaClear2.0 is co-funded by the European Union under the Horizon Europe Programme (Grant Agreement 101093822). Views and opinions expressed herein are those of the author(s) and do not necessarily reflect those of the European Union or European Climate, Infrastructure and Environment Executive Agency (CINEA). Neither the European Union nor the granting authority can be held responsible for them

defined as:

$$u^*(t) = -Kx(t) - K_r r \tag{52}$$

$$K = R^{-1}B^\top P_\infty \tag{53}$$

$$K_r = R^{-1}B^\top g_\infty \tag{54}$$

where computing P_∞ requires solving the algebraic Riccati equation:

$$A^\top P_\infty + P_\infty A - P_\infty B R^{-1} B^\top P_\infty + C^\top Q C = 0 \tag{55}$$

and g_∞ is defined as:

$$g_\infty = -((A - BR^{-1}B^\top P_\infty)^\top)^{-1} C^\top Q r \tag{56}$$

Note that since g_∞ depends on the reference r, each time the desired waypoint changes we need to recompute g_∞. Despite this fact, using the inifinite-horizon version of the LQT controll strategy still remains significantly cheaper than using the finite-horizon version, due to the fact that the feedback gain K is constant and the feedforward gain K_r changes only with the waypoint instead of at all time steps.

4.1.3 Simulations using the LQT control strategy

We validate the described infinite-horizon version of the LQT controller using the parameters of the BlueROV2 Heavy presented in [19]. The results obtained are presented in Figures 25 and 26. The desired trajectory for the experiment is constructed from a series of waypoints similar to the lawnmower used for the real experiments. Although the waypoints only vary the desired X and Y coordinates of the ROV, the trajectory reflects the fact that the dynamics of the ROV are not decoupled, since the change of the waypoint causes changes in the heave, roll and pitch of the ROV. By tuning the Q and R cost matrices, we designed a controller that handles the effect of these coupling effects according to our requirements, i.e. for detection and mapping purposes it focuses on accurately following the reference for the waypoints and on keeping the yaw of the ROV stable without large variation in roll and pitch.

4.1.4 Upgraded PID control

While developing the LQT control strategy, we kept working on improving PID control, this time with the goal of having better observations made by the ROV. First, to maintain a roughly constant distance from the litter for operating areas where the seafloor varies in depth, we updated the control so as to stabilize the altitude of the ROV above the seafloor to a constant reference (rather than stabilizing the depth as done in the original controller, which would allow distance to the litter to vary with the sea depth). Secondly, the yaw controller of the ROV was changed so that the robot aligns to the lawnmower instead of maintaining an independent orientation; specifically, the robot travels oriented perpendicularly to the longer legs of the lawnmower. Furthermore, we also retuned the parameters of the PID controller, and revised some transformations of the error signals from the world frame to the frame of the observation ROV.

Co-funded by the European Union

SeaClear2.0 is co-funded by the European Union under the Horizon Europe Programme (Grant Agreement 101093822). Views and opinions expressed herein are those of the author(s) and do not necessarily reflect those of the European Union or European Climate, Infrastructure and Environment Executive Agency (CINEA). Neither the European Union nor the granting authority can be held responsible for them

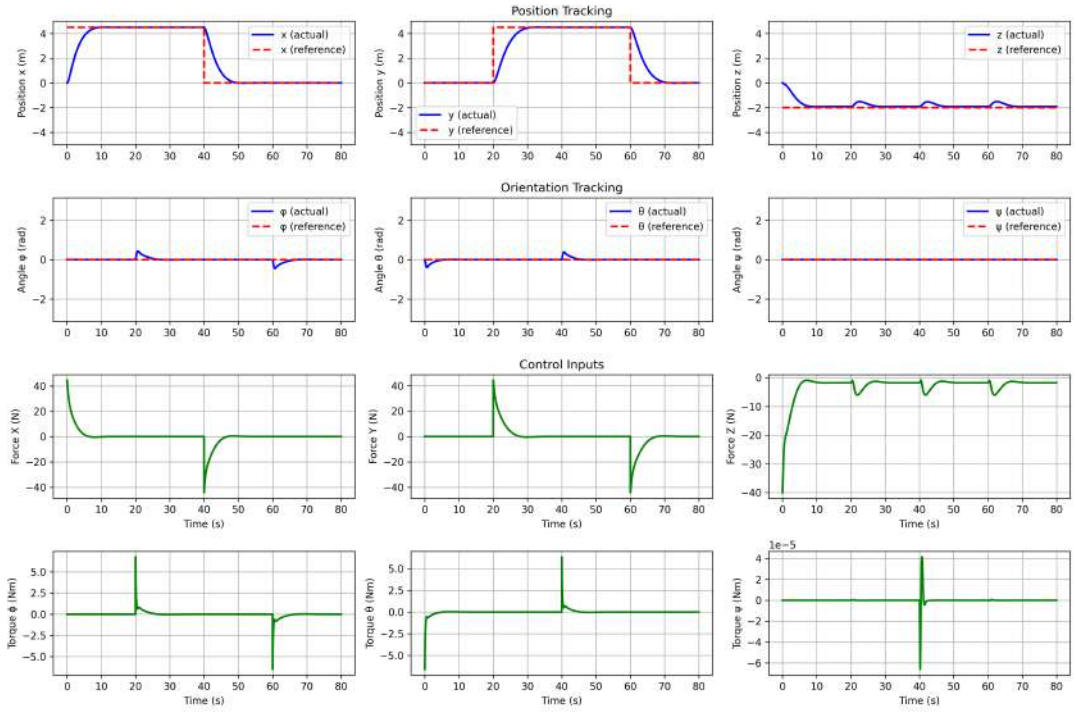


Figure 25: Simulation results using the infinite horizon LQT control strategy for the BlueROV2 Heavy model [19].

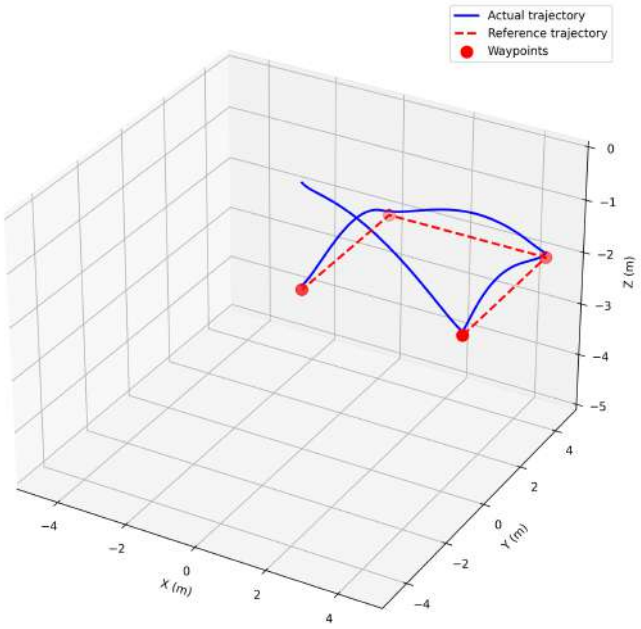


Figure 26: 3D visualisation of the results presented in Figure 25.

Co-funded by the European Union

SeaClear2.0 is co-funded by the European Union under the Horizon Europe Programme (Grant Agreement 101093822). Views and opinions expressed herein are those of the author(s) and do not necessarily reflect those of the European Union or European Climate, Infrastructure and Environment Executive Agency (CINEA). Neither the European Union nor the granting authority can be held responsible for them

4.1.5 Novel experimental results

In the end, given the main purpose of the ROV is to detect litter, the second set of control improvements – those of Section 4.1.4 – was deemed more important as it was geared towards better sensing. Therefore, we adopted this upgraded PID control for the latest system demonstration, in Dubrovnik. Figures 27 and 28 show recent control results during this demonstration. Outside a short interval without altitude-sensor data, the ROV manages to follow well the lawnmower trajectory while also stabilizing its altitude and following the required nonzero yaw reference.

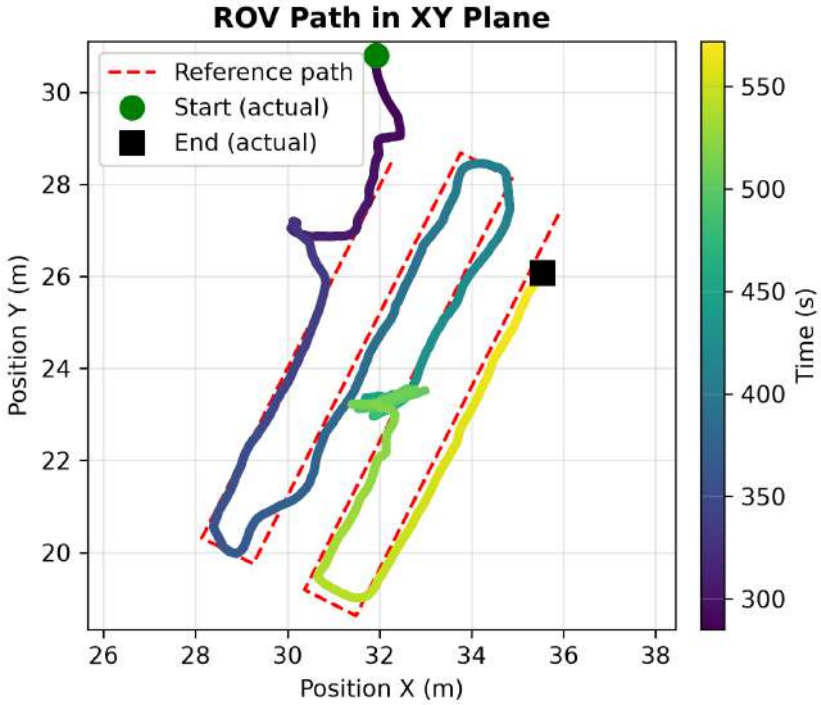


Figure 27: Automatic lawnmower trajectory run during the Dubrovnik demo using the upgraded PID controller. Note that robot starts some distance away from the lawnmower and must navigate to its first corner.

4.2 Underwater Smart Grapple

In SeaClear2.0, the function of the collection ROV is extended to the new USG. From a control perspective, the general structure of the control loops can be adapted for the USG, fitting the new kinematic and software structure. This section outlines the enhancements made to the control system, focusing on the integration of the low-level controller. Further details on the high-level control strategies and the coupled USV-USG control approach will be provided in the upcoming Deliverable 5.2, "Report on Smart Grapple Software Framework."

The smart grapple system retains several key similarities with the previous collection ROV:

- Cascaded Position and Velocity Control loops allow for separate tuning of position and velocity.

Co-funded by the European Union

SeaClear2.0 is co-funded by the European Union under the Horizon Europe Programme (Grant Agreement 101093822). Views and opinions expressed herein are those of the author(s) and do not necessarily reflect those of the European Union or European Climate, Infrastructure and Environment Executive Agency (CINEA). Neither the European Union nor the granting authority can be held responsible for them

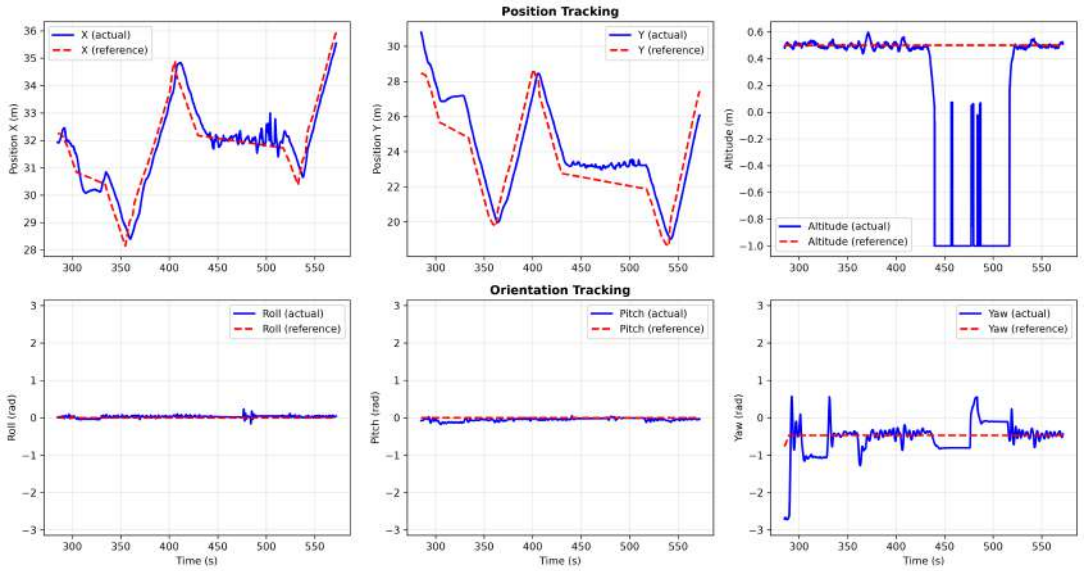


Figure 28: Per-DOF visualisation of the PID controller preformance during the lawnmower presented in Figure 27.

- Both systems use a standard ROV motion model. Compensation of inertia is enabled in feedforward components of the controllers. The motion model has been outlined in deliverable D4.2: "Report on Pose Estimation", Section 3.3.
- Neutrally Buoyant Design: The USG, like the ColROV, is neutrally buoyant with top buoyancy and a low center of mass, contributing to roll and pitch stability.
- Thruster Actuation: Both systems employ vectored thruster actuation, enabling precise maneuverability in underwater environments.

The smart grapple system introduces notable differences compared to the collection ROV:

- Fully Actuated System: Unlike the previously underactuated ColROV, the USG is fully actuated. This conditions a transition from 4 DOF to 6 DOF control, allowing active pitch and roll control.
- The control algorithms have been ported from ROS Noetic to ROS2 Humble Hawksbill to match the overall software architecture.

4.2.1 Cascaded PID Control Formulation

The cascaded PID control system consists of two controllers: a position controller and a velocity controller. The reference to the position controller is provided by the high-level guidance and navigation system of the USG, with the reference being either provided in a global frame using navigation information from the Short Baseline (SBL) underwater GPS, in a local body-fixed frame for relative motions, or the frame of the eye-in-hand camera for visual-servo tracking. The position controller generates a

Co-funded by the European Union

SeaClear2.0 is co-funded by the European Union under the Horizon Europe Programme (Grant Agreement 101093822). Views and opinions expressed herein are those of the author(s) and do not necessarily reflect those of the European Union or European Climate, Infrastructure and Environment Executive Agency (CINEA). Neither the European Union nor the granting authority can be held responsible for them

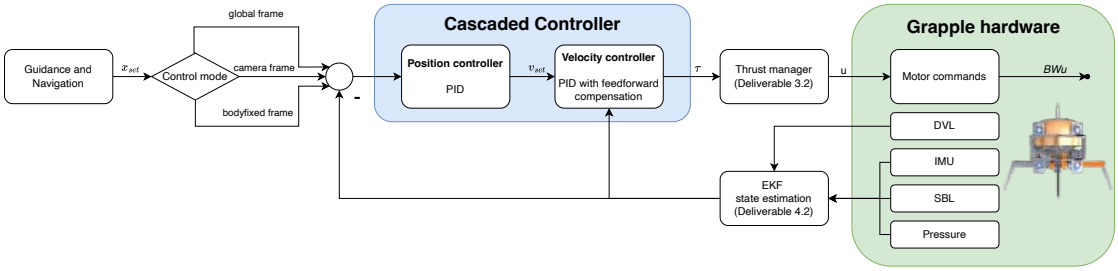


Figure 29: Low-level control loop for the smart grapple.

velocity setpoint, which is then used by the velocity controller to generate the control input τ as a 6 DOF wrench command to the thrust manager. Feedforward compensation is included in the velocity controller to account for mass inertia based on model information. Both controllers produce control inputs for the three translational and three rotational components of the full 6 DOF workspace, under the assumption of the individual DOFs being sufficiently decoupled to neglect motion interference between DOFs as disturbance. The resulting low-level control loop is illustrated in Figure 29. Please note that the thruster manager for constrained thrust allocation has been described in deliverable D3.2: "Smart Grapple Design Report" and the Extended Kalman Filter (EKF) filter structure has been presented in D4.2: "Report on Pose Estimation".

The position controller can be formulated as:

$$v_{set}(t) = K_{p1} e_p(t) + K_{i1} \int_0^t e_p(\tau)\, d\tau + K_{d1} \frac{de_p(t)}{dt} \tag{57}$$

where:

- $v_{set}(t)$ is the velocity setpoint.
- $e_p(t) = x_{set}(t) - x(t)$ is the position error.
- K_{p1} is the proportional gain, K_{i1} is the integral gain and K_{d1} is the derivative gain for the position controller.

The subsequent velocity controller can be formulated as:

$$\tau(t) = K_{p2} e_v(t) + K_{i2} \int_0^t e_v(\tau)\, d\tau + K_{d2} \frac{de_v(t)}{dt} + m\ddot{x}(t) \tag{58}$$

where:

- $\tau(t)$ is the control input to the thrust manager as a wrench command per DOF.
- $e_v(t) = v_{set}(t) - \dot{x}(t)$ is the velocity error.
- K_{p2} is the proportional gain, K_{i2} is the integral gain and K_{d2} is the derivative gain for the velocity controller.

Co-funded by the European Union

SeaClear2.0 is co-funded by the European Union under the Horizon Europe Programme (Grant Agreement 101093822). Views and opinions expressed herein are those of the author(s) and do not necessarily reflect those of the European Union or European Climate, Infrastructure and Environment Executive Agency (CINEA). Neither the European Union nor the granting authority can be held responsible for them

- m is the mass of the grapple.
- $\ddot{x}(t)$ is the acceleration of the system.

4.2.2 Simulations

We evaluate the architecture shown in Figure 29 in the Marine Robotic Unity Simulator using a set of representative simple scenarios:

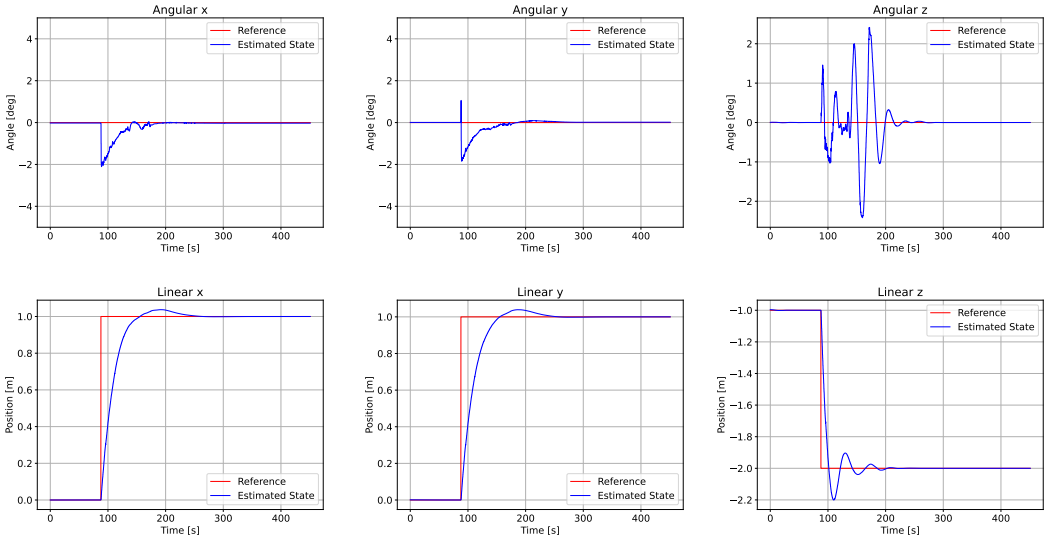


Figure 30: Pure translation from $\{0, 0, -1, 0, 0, 0\}$ to $\{1, 1, -2, 0, 0, 0\}$.

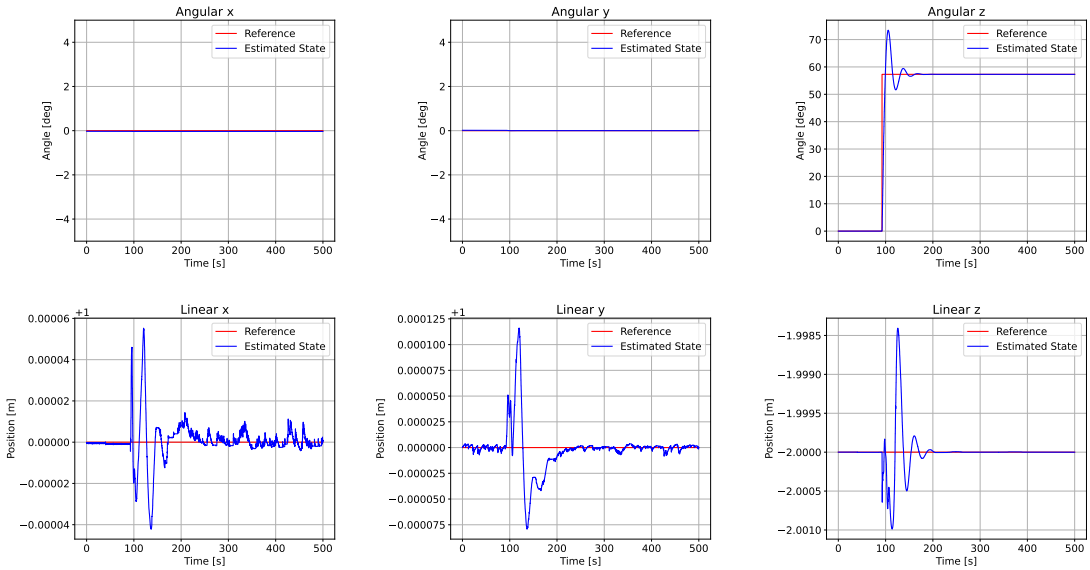


Figure 31: Pure rotation from $\{1, 1, -2, 0, 0, 0\}$ to $\{1, 1, -2, 0, 0, 57.296°\}$.

Co-funded by the European Union

SeaClear2.0 is co-funded by the European Union under the Horizon Europe Programme (Grant Agreement 101093822). Views and opinions expressed herein are those of the author(s) and do not necessarily reflect those of the European Union or European Climate, Infrastructure and Environment Executive Agency (CINEA). Neither the European Union nor the granting authority can be held responsible for them

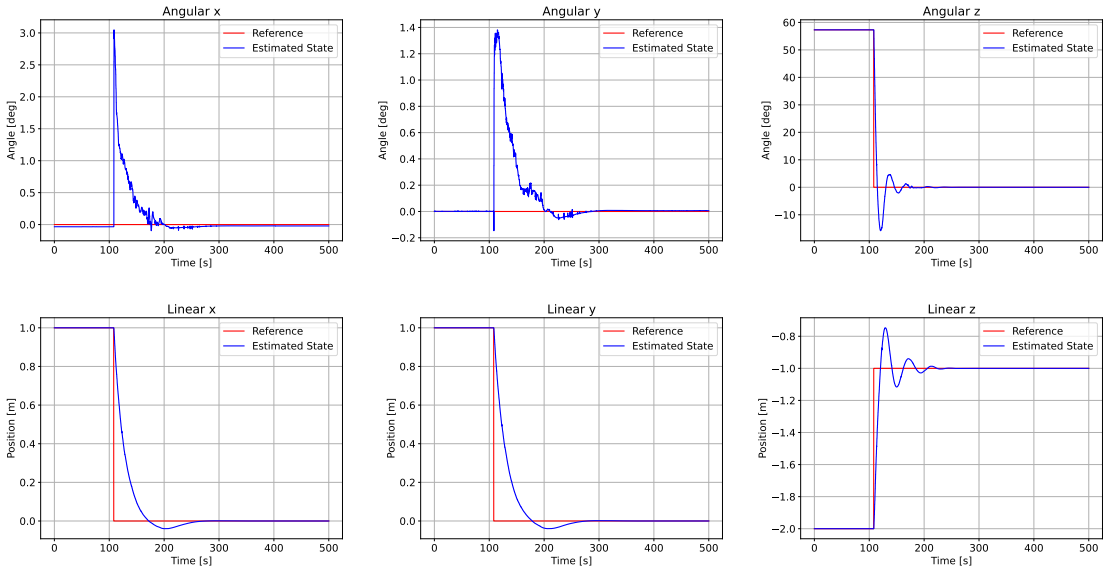


Figure 32: Mixed translation & rotation from $\{1, 1, -2, 0, 0, 57.296°\}$ back to $\{0, 0, -1, 0, 0, 0\}$.

The cascaded PID controller's performance was evaluated through step response analysis in three distinct test cases, with the results presented in Figures 30 to 32. In the *pure-translation test*, the smart grapple three translational axes demonstrated a smooth convergence to the 1m setpoint, with only a modest overshoot. Despite some larger yaw (z-axis) oscillations at the beginning of the maneuvers, the attitude of the grapple remained stable around $0°$. The *pure-rotation* experiment highlighted the system's decoupling capabilities. The yaw axis accurately tracked a $\approx 57°$ step input with no discernible steady-state error, while the roll, pitch, and translational channels showed minimal deviation from their initial states. This behavior is characteristic of cascade control systems where the inner loop dynamics are significantly faster than those of the outer loop (cf. gains in Tables 4 and 5). In the combined *translation-rotation* test, a final reference command was issued to return the grapple to its initial configuration, effectively reversing the previous two maneuvers. While minor oscillations emerged, all channels settled to their respective setpoints with negligible steady-state error. This outcome validates the efficacy of the selected PID gains (Tables 4 and 5) in providing sufficient damping and integral action for both position and attitude control. These parameters must still be tested in real-world experiments and could be further improved through controller tuning.

4.2.3 Experimental results

We demonstrate performance of the integrated control cascade with velocity trajectory generation from the visual servoing approach (outlined in D5.2). The control objective is to center the bounding box within the onboard camera's horizontal frame and reach the desired altitude (pose) vertically using the Doppler Velocity Logger (DVL) feedback. Once the desired pose is achieved, the state machine transitions to the grasping state.

Experimental data from the Dubrovnik trials in June 2026 is shown in Figures 33 and 34. The selected sequence corresponds to an autonomous visual-servoing approach towards a tire target. During the

Co-funded by the European Union

SeaClear2.0 is co-funded by the European Union under the Horizon Europe Programme (Grant Agreement 101093822). Views and opinions expressed herein are those of the author(s) and do not necessarily reflect those of the European Union or European Climate, Infrastructure and Environment Executive Agency (CINEA). Neither the European Union nor the granting authority can be held responsible for them

The gains of the cascaded controller in Figure 29 were tuned in simulation and set as follows:

Table 4: Velocity-controller gains

Axis	P	I	D
Linear x	100.0	0.0	0.0
Linear y	100.0	0.0	0.0
Linear z	200.0	0.0	0.0
Angular x	1.0	0.0	0.0
Angular y	1.0	0.0	0.0
Angular z	1.0	0.0	0.0

Table 5: Position-controller gains

Axis	P	I	D
Linear x	0.3	0.1	0.2
Linear y	0.3	0.1	0.2
Linear z	0.3	0.1	0.2
Angular x	1.0	0.2	0.2
Angular y	1.0	0.2	0.2
Angular z	1.0	0.1	0.2

shown interval, the tire remains in the onboard camera view, controller-level visual-servoing commands are active, the DVL velocity estimates indicate vehicle motion, and the DVL altitude decreases as the Grapple approaches the target.

Co-funded by the European Union

SeaClear2.0 is co-funded by the European Union under the Horizon Europe Programme (Grant Agreement 101093822). Views and opinions expressed herein are those of the author(s) and do not necessarily reflect those of the European Union or European Climate, Infrastructure and Environment Executive Agency (CINEA). Neither the European Union nor the granting authority can be held responsible for them

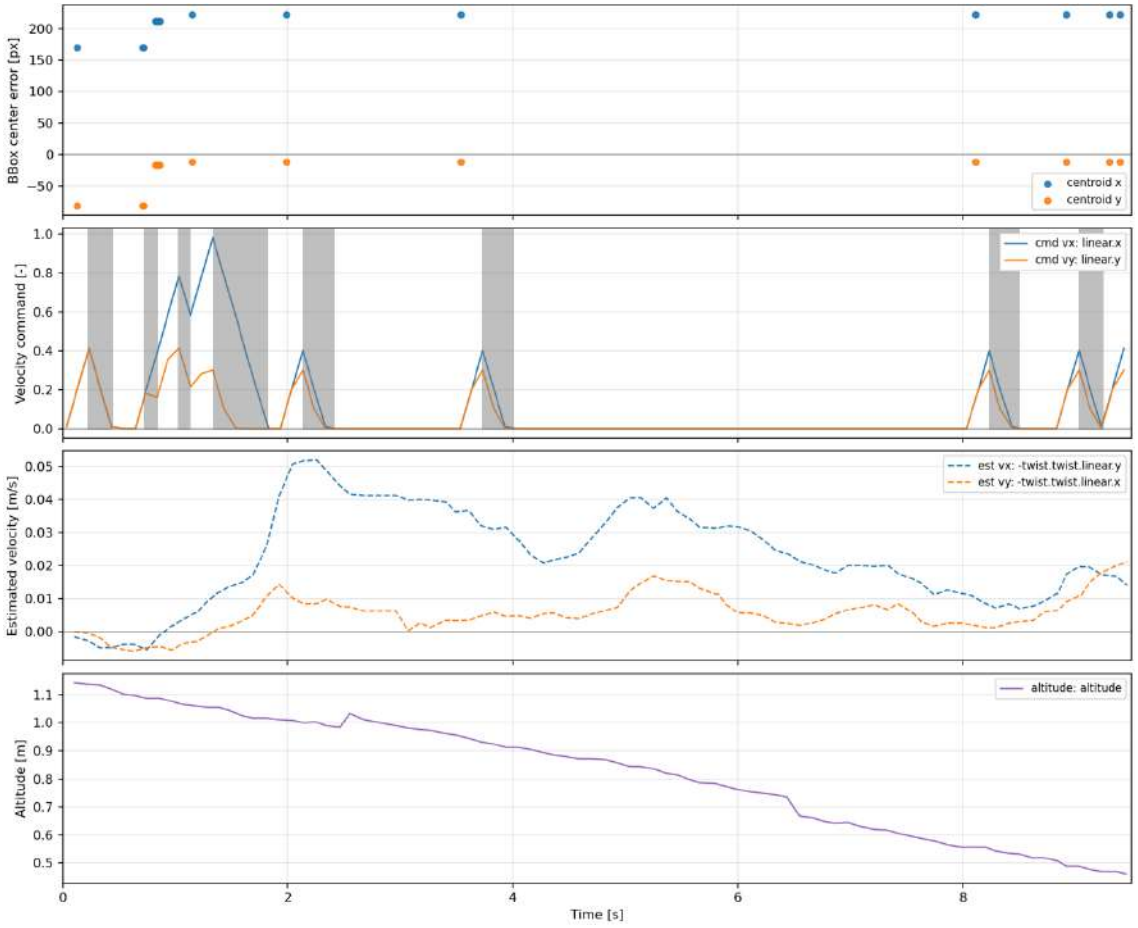


Figure 33: Experimental visual-servoing data from a successful tire approach. The plots show a bag-relative time window with the time axis reset to zero. From top to bottom: image-plane bounding-box centroid error, controller-level console commands, velocity estimates, and DVL altitude. The centroid-error axes follow the camera image convention, while the controller commands follow the controller convention; in this experiment, positive centroid-x error corresponds to positive x command action, whereas positive centroid-y error corresponds to negative y command action. The gray shaded intervals indicate periods where the last active command is gradually decayed, in order to reduce sensitivity to intermittent detections and transient false positives.



Figure 34: OAK-D RGB frames extracted from the same visual-servoing interval as Figure 33, ordered left-to-right and top-to-bottom. The sequence shows the tire moving through the camera field of view while the USG approaches the target.

Co-funded by the European Union

SeaClear2.0 is co-funded by the European Union under the Horizon Europe Programme (Grant Agreement 101093822). Views and opinions expressed herein are those of the author(s) and do not necessarily reflect those of the European Union or European Climate, Infrastructure and Environment Executive Agency (CINEA). Neither the European Union nor the granting authority can be held responsible for them

5 Conclusion

This report detailed the methodologies and advancements in control techniques for the SeaClear 2.0 project, focusing on Unmanned Surface Vehicles (USVs), Remotely Operated Vehicles (ROVs), and the Unmanned Aerial Vehicles (UAV). The integration of control techniques - specifically the Model Predictive Control (MPC), cascaded Proportional Integral Derivative (PID) and Linear Quadratic Tracking (LQT) - significantly enhanced the accuracy and reliability of control performance across these heterogeneous robotic platforms. Both experimental and simulation results indicate the effectiveness of the proposed techniques in practical scenarios. Promising simulation outcomes were observed for the MiniTortuga ROV proposed LQT control technique as well as for the MPC - based cooperative control of the SeaBees, with experimental validation planned as the next step for both. For the SeaCat2 USV, an MPC-based DP controller has been proposed and is slated for experimental validation. Furthermore, simulated tests within the MArine Robotic Unity Simulator (MARUS) demonstrated the efficacy of the cascaded PID control architecture for the Underwater Grapple System (USG). Through a series of experiments the effectiveness of the proposed control for tethered UAV was demonstrated. In summary, the advancements in control techniques detailed in this report establish a robust foundation for the continued development and deployment of autonomous robotic systems, particularly for marine litter collection within the SeaClear 2.0 initiative and for autonomous systems in general.

Co-funded by the European Union

SeaClear2.0 is co-funded by the European Union under the Horizon Europe Programme (Grant Agreement 101093822). Views and opinions expressed herein are those of the author(s) and do not necessarily reflect those of the European Union or European Climate, Infrastructure and Environment Executive Agency (CINEA). Neither the European Union nor the granting authority can be held responsible for them

References

[1] V. Prkačin, I. Palunko, and I. Petrović, "State and parameter estimation of suspended load using quadrotor onboard sensors," in *2020 International Conference on Unmanned Aircraft Systems (ICUAS)*, 2020, pp. 958–967.

[2] V. Prkačin, I. Palunko, and I. Petrović, "Extended kalman filter for payload state estimation utilizing aircraft inertial sensing," in *2021 Aerial Robotic Systems Physically Interacting with the Environment (AIRPHARO)*, 2021, pp. 1–6.

[3] M. Tognon and A. Franchi, *Theory and Applications for Control of Aerial Robots in Physical Interaction Through Tethers*, ser. Tracts in Advanced Robotics. Springer, 2020.

[4] *Model Predictive Control Toolbox R2022a*, The Mathworks, Inc., 2022. [Online]. Available: https://www.mathworks.com/help/mpc/

[5] *DJI M210 RTK V2 Manual*, DJI, 2019. [Online]. Available: https://www.dji.com/hr/matrice-200-series-v2/info

[6] *DJI Onboard SDK (OSDK) 4.1.0*, DJI, 2021. [Online]. Available: https://github.com/dji-sdk/Onboard-SDK

[7] V. Prkačin, A. Duraš, and I. Palunko, "Coordinated control of tethered unmanned aerial vehicle with launch and recovery system," in *2024 International Conference on Smart Systems and Technologies (SST)*, 2024, pp. 293–298.

[8] V. Prkačin, I. Palunko, and I. Petrović, "Trajectory tracking and tether tension control of tethered aerial vehicle using nonlinear model predictive control," *Control Engineering Practice*, 2025 - to be published.

[9] T. I. Fossen, *Handbook of Marine Craft Hydrodynamics and Motion Control*. John Wiley & Sons, 2011.

[10] T. I. Fossen and T. Perez, "MSS (Marine Systems Simulator)," https://github.com/cybergalactic/MSS, 2004.

[11] T. I. Fossen, *Guidance and Control of Ocean Vehicles*. John Wiley & Sons, 1994.

[12] O. M. Faltinsen, *Hydrodynamics of High-Speed Marine Vehicles*. Cambridge University Press, 2006.

[13] ——, *Hydrodynamics of High-Speed Marine Vehicle*. Cambridge University Press, 2005.

[14] R. Skjetne, O. Smogeli, and T. Fossen, "A nonlinear ship manoeuvering model: Identification and adaptive control with experiments for a model ship," *Modeling, Identification and Control*, vol. 25, pp. 3–27, 2004.

[15] T. I. Fossen, *Marine control systems: guidance. navigation, and control of ships, rigs and underwater vehicles*. Marine Cybernetics, Trondheim, Norway, Org. Number NO 985 195 005 MVA, www. marinecybernetics. com, ISBN: 82 92356 00 2, 2002.

Co-funded by the European Union

SeaClear2.0 is co-funded by the European Union under the Horizon Europe Programme (Grant Agreement 101093822). Views and opinions expressed herein are those of the author(s) and do not necessarily reflect those of the European Union or European Climate, Infrastructure and Environment Executive Agency (CINEA). Neither the European Union nor the granting authority can be held responsible for them

[16] K. D. Do and J. Pan, *Control of Ships and Underwater Vehicles*, ser. Advances in Industrial Control. Springer London, 2009. [Online]. Available: http://link.springer.com/10.1007/978-1-84882-730-1

[17] C. Delea, "D3.3: Shuttle tender usv hardware design report," Fraunhofer, Tech. Rep., 6 2024. [Online]. Available: https://www.seaclear2.eu/project-deliverables/

[18] ——, "D5.3: Report on tender usv autonomous operation," Fraunhofer, Tech. Rep., 12 2025. [Online]. Available: https://www.seaclear2.eu/project-deliverables/

[19] C.-J. Wu, "6-dof modelling and control of a remotely operated vehicle," Ph.D. dissertation, Flinders University, College of Science and Engineering., 2018.

[20] F. L. Lewis, D. Vrabie, and V. L. Syrmos, *Optimal control*. John Wiley & Sons, 2012.

Co-funded by the European Union

SeaClear2.0 is co-funded by the European Union under the Horizon Europe Programme (Grant Agreement 101093822). Views and opinions expressed herein are those of the author(s) and do not necessarily reflect those of the European Union or European Climate, Infrastructure and Environment Executive Agency (CINEA). Neither the European Union nor the granting authority can be held responsible for them